INTERNATIONAL ATOMIC ENERGY AGENCY
UNITED NATIONS EDUCATIONAL, SCIENTIFIC AND CULTURAL ORGANIZATION
INTERNATIONAL CENTRE FOR THEORETICAL PHYSICS
I.C.T.P., P.O. BOX 586, 34100 TRIESTE, ITALY, CABLE CENTRATOM TRIESTE

H4-SMR 393/23

SPRING COLLEGE ON PLASMA PHYSICS

15 May - 9 June 1989

CAVITON DYNAMICS IN STRONG LANGMUIR TURBULENCE

D. Du Bois

Los Alamos National Laboratory
P.O.Box 1663
Ns H828 Lani
New Mexico
Los Alamos 87545
U.S.A.

Caviton Dynamics in Strong Langmuir Turbulence*

Don DuBois, Harvey A. Rose and David Russell
Theoretical Division and Center for Nonlinear Studies**
Los Alamos National Laboratory, Los Alamos, NM, 87545

Recent studies based on long time computer simulations of Langmuir turbulence as described by Zakharov's model will be reviewed. These show that for strong to moderate ion sound damping the turbulent energy is dominantly in nonlinear "caviton" excitations which are localized in space and time. A local caviton model will be presented which accounts for the nucleation-collapse-burnout cycles of individual cavitons as well as their space-time correlations. This model is in detailed agreement with many features of the electron density fluctuation spectra in the ionosphere modified by powerful HF waves as measured by incoherent scatter radar. Recently such observations have verified a prediction of the theory that "free" Langmiur waves are emitted in the caviton collapse process. These observations and theoretical considerations also strongly imply that cavitons in the heated ionosphere, under certain conditions, evolve to states in which they are ordered in space and time. The sensitivity of the high frequency Langmuir field dynamics to the low frequency ion density fluctuations and the related caviton nucleation process will be discussed.

*Paper for presentation at the International Centre for Theoretical Physics, Spring College on Plasma Physics "Large Amplitude Waves and Fields in Plasmas" 22-26 May, 1989, Trieste, Italy.

**Research supported by USDOE.

I. INTRODUCTION

In this lecture I want to summarize the results of a research program which has focused on the "long time" development of strong Langmuir turbulence (SLT) which is driven by intense coherent radiation in long scale length plasmas near critical density. This problem was chosen for its theoretical simplicity and because of its relevance to ionospheric modification experiments using powerful HF radiation. These experiments probably provide the best physical realization of the theoretical ideal, long scale length, quasi stationary plasma.

The strong Langmuir turbulent system which I will try to describe is a fascinating system in which locally coherent, nonlinear "wave" structures or excitations undergo chaotic or turbulent motion. These elementary excitations which we call "cavitons" consist of high frequency Langmuir waves trapped in self-consistently evolving density cavities. The low frequency density response which describes the cavities evolves under the influence of the pondermotive force of the localized Langmuir waves. These excitations have a finite lifetime; they are born by gaining energy from the external fields in a process of "nucleation;" they "collapse" to small dimensions where they die or "burnout" by giving up their electrostatic energy to accelerated electrons. These excitations also interact by the radiation of ion acoustic waves and "free" Langmuir waves. The study of this interaction is in its infancy but we have examples in which the caviton gas apparently undergoes a phase transition to states which are highly ordered in space and time. These phenomena are a significant departure from our concepts of linear wave excitations and weak turbulence or renormalized turbulence theories with their often uncontrolled assumptions such as random phase approximations.

Data from the ionospheric modification experiments has accumulated for about 15 years. In the early days these data seemed consistent with the conventional theory involving linear parametric instabilities and weak turbulence cascades. However, with the passage of time it was realized that these data were manifestly inconsistent with the conventional theory. A more detailed discussion of this is given in reference 1 from which much of the material here is derived.

During the same time period new theoretical insights into SLT were developed centering around the seminal work of V. E. Zakharov.[2] He developed a very useful

unified description of SLT and concluded that collapsing localized Langmuir states would play a central role in the turbulent state. In recent years it has been possible to carry out long time computer simulations of Zakharov's model equations in two[3,4] and three[5] spatial dimensions. We believe our work has led to a new set of paradigms for the understanding of SLT and its application to the ionospheric modification experiments.[1]

The results of this research can be summarized as follows:

1.) States of SLT can be excited for heater (pump) intensities only marginally above the threshold for parametric instabilities. Thus we expect the ionospheric heating experiments, which are estimated to be well above the threshold for these parametric instabilities will be in the SLT regime.

2.) In these states of SLT a major part of the power in high frequency density fluctuations is contained in localized states in the case of strong ion sound wave damping which is appropriate to the ionosphere.[1,3,4] These localized states, which we will call cavitons, consist of a high frequency Langmuir field trapped in a self-consistent density cavity (i.e., density depletion). The dynamics of these cavitons will be a major concern of this paper. It is important to emphasize that these localized states are not wavepackets of plane linear Langmuir waves, but new nonlinear Langmuir states and consequently cannot be described by perturbation arguments such as weak turbulence theory based plane wave states.

3.) This state of SLT is sustained by a local nucleation process, (see 6. below), and not by linear parametric instabilities.[3,6,7] The developed turbulent state is stable to the excitation of these global parametric processes because of the level and localized nature of the turbulent fluctuations. Parametric instabilities may play a role in the transient excitation of the SLT state from quiescent initial conditions; for ionospheric parameters this would be the first few ms following the turn-on of the heater.

4.) The localized states are trapped in self-consistently evolving density wells which collapse to small dimensions because of the dominance of the nonlinear pondermotive force over the linear pressure force. The evolution from nucleation to collapse is discussed by Rose and Weinstein[8] and the collapse process follows the self-similar scaling discussed by several Soviet authors.[2,9]

5.) As the caviton's spatial dimension decreases to the order of 5-10 electron Debye lengths, λ_{De}, the electrostatic energy trapped in the caviton is rapidly given

up in the acceleration of electrons resulting in the sudden dissipation or "burnout" of electrostatic energy.

6.) The electrostatic burnout process leaves an empty density cavity, no longer supported by a pondermotive force, which then evolves as a free ion sound pulse. These residual ion density wells provide nucleation centers for the excitation of new collapsing cavitons.[3,6,7] For strong ion sound damping, appropriate to the ionosphere, the burnout density wells relax in place.

One purpose of this paper is to review several years of research on strong Langmuir turbulence. Highlights of this research have been reported in several short articles.[3,4,6,7] Limiting the scope of this discussion to ionospheric heating greatly reduces the "volume" of the potentially very large parameter space of SLT which is considered, although what remains is still very rich in phenomena. Other applications such as laser-plasma interactions (e.g., see Rose, DuBois and Bezzerides[10,11] involve many of the same or related phenomena. The same conditions of excitation near the critical density in weak density gradients might be approximated in long scale length laser produced plasmas with weak collisionality or in laboratory microwave-plasma experiments with sufficiently long-lived plasmas uneffected by boundaries. We will not treat such applications in detail here.

A second purpose of this paper is to sketch out the application of this strong turbulence scenario, which we believe represents the most credible description of Langmuir turbulence, to the experimental facts of ionospheric heating. This SLT approach represents a significant departure from the accepted or conventional ideas associated with parametric instabilities and weak turbulence cascades.

Our most complete current understanding of SLT is based on simulations of a homogeneous, isothermal model described by Zakharov's [1972] equations.[2] This situation is best realized in ionospheric modification for early times (several ms) after heater turn on before large scale (several m) density and temperature fluctuations have had time to develop. The most relevant data for this situation seems to be that obtained by Wong et al.,[12] Djuth et al.[13] and recently by Cheung et al.[14] in low duty cycle pulsed heating of the ionosphere.

A more detailed comparison of the SLT theory to ionospheric modification experiments is given in reference 1.

2. ZAKHAROV'S MODEL OF NONLINEAR LANGMUIR WAVE-ION SOUND WAVE INTERACTIONS

The calculations to be reported here will be based on solutions of Zakharov's [1972] model[2] of Langmuir wave-ion sound wave interactions. These are formulated in terms of the slowly time varying envelope field $\underline{\tilde{E}}(\underline{x},t)$ of the total electrostatic field $\underline{E}_{TOT}(\underline{x},t)$, where

$$\underline{E}_{TOT}(\underline{x},t) = \frac{1}{2}\underline{\tilde{E}}(\underline{x},t)exp[-i\omega_p t] + c.c \tag{2.1}$$

where $\omega_p^2 = 4\pi^2 n_0/m_e$ where n_0 is the mean plasma electron density. It is assumed that

$$|\partial_t \underline{\tilde{E}}| << |\omega_p \underline{\tilde{E}}| \,. \tag{2.2}$$

The total ion density is written as

$$n_{TOT} = n_0 + \tilde{n} \tag{2.3}$$

where $\tilde{n}$ is the fluctuation about the mean density; the spatial average of $\tilde{n}$ is then zero.

The equations of Zakharov's model are:

$$\underline{\nabla}\cdot\left[(i\partial_t + \nu_e\bullet) + \frac{3}{2}\,\omega_p\lambda_D^2\nabla^2 - \frac{1}{2}\,\frac{\tilde{n}}{n_o}\,\omega_p\right]\underline{\tilde{E}} = \underline{\tilde{E}}_0\cdot\underline{\nabla}\left[\frac{\tilde{n}}{2n_0}\,\omega_p\right] \tag{2.4a}$$

$$\left[\partial_t^2 + 2\nu_i\bullet\partial_t - c_s^2\nabla^2\right]\tilde{n} = \frac{1}{16\pi m_i}\,\nabla^2|\underline{\tilde{E}} + \underline{\tilde{E}}_0|^2 \tag{2.4b}$$

where $\underline{\nabla}\times\underline{\tilde{E}} = 0$. Here λ_D is the electron Debye length and $c_S = (\eta\, T_e/m_i)^{1/2}$ is the ion acoustic speed which is often expressed in terms of specific heat parameters. $\underline{\tilde{E}}_0$ is the possibly time-dependent pump which is assumed to be spatially uniform. This is the "heater" field in ionspheric modification experiments. Tildes are used to denote conventional dimensional quantities to distinguish them where necessary from dimensionless quantities introduced below.

The damping operators $\tilde{\nu}_e\bullet$ and $\tilde{\nu}_i\bullet$ which are nonlocal in coordinate space are local in Fourier space. In Fourier space it is also simple to include a weak background geomagnetic field $\underline{B}_0$ based on the modified Bohm-Gross dispersion relation for Langmuir waves.[15]

$$\omega(k)^2 = \omega_p^2 + 3k^2v_e^2 + \omega_c^2 sin^2\,\theta \tag{2.5}$$

where $v_e^2 = T_e/m_e$, $\omega_c = e\,B_o/mc$ and θ is the angle between $\underline{B}_o$ and $\underline{k}$.

In this paper we adopt the convention for spatial Fourier transforms:

$$E(\underline{k}) = (L)^{-D}\int d^D x\; exp[-i\underline{k}\cdot\underline{x}]E(\underline{x}) \tag{2.6}$$

where L is the linear dimension of the system and D is the dimensionality of space.

The ionospheric heater or "pump" field $\underline{\tilde{E}}_0(t)$ is included, ignoring pump depletion, by assuming that the spatially uniform, k = 0, Fourier component is a given function $\underline{\tilde{E}}(t)$. We will generally take $\underline{\tilde{E}}_0(t)=\underline{\tilde{E}}_0\,exp\,[-i\tilde{\omega}_0 t]$ where $\tilde{\omega}_0=\omega_H - \omega_p$ is the difference between the heater frequency and the average plasma frequency.

The Langmuir wave dumping term is taken to be collisional damping plus Landau damping.

$$\tilde{\nu}_e(\tilde{k})\omega_p = \tilde{\nu}_c/\omega_p + \sqrt{\pi/8}\epsilon^{-3/2}(k_D/\tilde{k})^3 exp - (k_D^2/2\tilde{k}^2) \tag{2.7}$$

for $\tilde{k} < 0.3k_D$; this function is continued smoothly to increase as $\tilde{k}^2$ for large $\tilde{k}$. The latter step is necessary in order to arrest collapse at small scales as discussed by Zakharov and Shur[16] and Russell et al.,[3,7] it is essential for numerical resolution. This damping is an ad hoc addition to the model which is justified by comparing with particle in cell simulations.[17,18,19,20] which show nearly complete dissipation of the trapped electrostatic field at the burnout stage of collapse. For the work reported here, where we treat heater intensities well above the collisional thresholds for parametric instabilities, we will take $\tilde{\nu}_c = 0$. This is valid provided all physically important rates are much larger than ν_c.[1]

For ionospheric conditions we expect the ratio of electron to ion temperatures, T_e/T_i, to be of order unity for early times after the onset of heating. Fluid description of the ion density response is then expected to be quantitatively inaccurate

because of the important role of Landau damping on ions.[21] Since kinetic simulations of the ion response are prohibitively expensive for the problems we treat here we have adopted the following strategy: We use the fluid description of (2.4b) but the sound velocity c_S and the ion Landau damping used in this equation are chosen to coincide with the least damped poles of the linear kinetic response. Using this procedure we find for $\tilde{k} << k_{D_e}$ that $\tilde{\nu}_i(\tilde{k})/\tilde{\omega}_i(\tilde{k}) = \nu_i$ where $\tilde{\omega}_i(k) = \tilde{k}(\eta\ T_e/m_i)^{1/2}$. The values of ν_i and η are found from the least damped roots of the full kinetic dispersion relation.[1]

We have found the qualitative features of the nucleation process to be unaffected by the values of ν_i in the regime $0.9 > \nu_i > 0.4$ for systems driven well above the nucleation threshold discussed in Sec. 3.

It is well-known,[2] that the linearized form of these equations contains the parametric decay instability (PDI)[22] and modulational instability[23,24] (MI or OTSI) of the pump wave. Furthermore, when weak turbulence analysis[25,26] is applied to these equations it yields the usual wave kinetic type of equations which lead to the weak turbulence cascade. However, the validity conditions for the weak turbulence approximations are very limiting.[26]

We have studied examples of the solution of these equations for parameters relevant to ionosphere heating in which the system is initially excited by a linear parametric instability and evolves to a state of SLT.[1] In this paper, however, we will consider only the developed turbulent state.

In carrying out numerical solutions of these equations it is convenient to use dimensionless untilded quantities which are related to dimensional tilded quantities in the following way:[25]

$$t \equiv \frac{2}{3}\left(\eta\frac{m_e}{m_i}\right)\omega_p\tilde{t}$$

$$X \equiv \frac{2}{3}\left(\eta\frac{m_e}{m_i}\right)^{1/2}\frac{\tilde{x}}{\lambda_D} \tag{2.8}$$

$$E = \frac{1}{\eta^{1/2}}\left(\frac{m_i}{\eta m_e}\right)^{1/2}\left(\frac{3}{16\pi}\,\frac{\tilde{E}^2}{4\pi n_0 T_e}\right)^{1/2}$$

The scaled equations then have the familiar simple form

$$\underline{\nabla}\cdot[i(\partial_t + \nu_e\bullet) + \nabla^2 - n]\underline{E} = \underline{E}_0\cdot\underline{\nabla}n \tag{2.9a}$$

$$[\partial_t^2 + 2\nu_i\bullet\partial_t - \nabla^2]n = \nabla^2|\underline{E} + \underline{E}_0|^2 \tag{2.9b}$$

In the scaled units there is a residual mass ratio dependence which occurs only in the scaled damping rate which is obtained from (2.7) as follows:

$$\nu_e(k) = (3/2)M\tilde{\nu}_e(2/3M^{-1/2}k k_D)\omega_p^{-1} \tag{2.10}$$

in terms of the scaled wavenumber k and $M = m_i/\eta m_e$. This residual mass ratio dependence reflects the ratio of the parametric instability space and time scales which increase with M and the mass ratio independent dissipation scale. A similar formula applies to $\nu_i(k)$.

Note that in dimensional units Landau damping becomes significant for $\tilde{k} > 0.2k_D(k_D = \lambda_D{}^{-1})$. Thus in dimensionless units this dissipation becomes significant for k greater than the dissipation scale k_d:

$$k > k_d \simeq (0.2)\cdot\ \frac{3}{2}\left(\frac{m_i}{\eta m_e}\right)^{1/2}$$

Since the dynamics of the decay instability involves $\tilde{k}$'s on the scale of $\tilde{k}_* = (2/3)(\eta m_e/m_i)^{1/2}\ k_D$ we need Fourier components at least as small as this, if the parametric processes are important, and this sets the linear dimension of the simulation cell to be $\tilde{L}_x = \tilde{L}_y > 2\pi/k_*$. In dimensionless units $k_* = 1$ and $L_x = L_y > 2\pi$. The number of Fourier modes must be sufficient to probe deep within the dissipation range of $k_{max} >> k_d$ in order to resolve collapse. This sets a limit on the value of M which can be accommodated in a reasonably sized simulation of say 128 × 128 Fourier modes in two dimensions. In view of these limitations we have chosen M = 1836 for our simulations. At various points in the text to follow, especially in Section 3, we will discuss the scaling of physical quantities with the mass ratio. This scaling will allow us, at least roughly, to translate the simulation results to the larger mass ratios.

The validity conditions for Zakharov's model have been discussed elsewhere (Zakharov[1972] Nicholson [1983]) and include the condition.

$$\frac{|\tilde{E}|^2}{4\pi n_0 T_e} << 1 \qquad (2.11a)$$

$$\frac{\tilde{n}}{n_0} << 1 \qquad (2.11b)$$

A discussion of the degree to which these conditions are satisfied in our numerical simulations is given in reference 1.

Our simulations are carried out on a 128 x 128 square grid of sides $L_x = L_y = 2\pi$, with periodic boundary conditions in x and y. In physical units this implies $L_x = L_y = 404\ \lambda_{D_e}$ and a grid-point spacing $\Delta x = \Delta y = 3.15\ \lambda_{D_e}$. The Debye wavenumber in these units is 64.3 and the maximum wavenumber is 91. Spot checks with a dealiased code with a nominal 256 x 256 grid were used to confirm the validity of our simulations. Typically the spectrum ($|n(k)|^2$) decreases by 4 orders of magnitude between the peak of the spectrum and the largest k values. The test of temporal and spatial resolution is energy conservation as expressed by the balance between the average dissipation and injection rates as discussed in Sec. 4.

3. THE LOCAL CAVITON MODEL

The accumulated evidence from many computer simulations of equations (2.4) shows that, at least for moderate to strong ion acoustic wave damping, $\nu_i \gtrsim 0.1$, the strongly turbulent system is dominated by caviton "events" which are localized in space and time. Snapshots such as Figure 1 show the localized nature of $|\underline{E}(\underline{x},t)|^2$ and $n(\underline{x},t)$ as functions of $\underline{x}$ for given t. The power spectra $|\underline{E}(\underline{k},\omega)|^2$, which we will discuss in detail below, also have signatures of localized states. The envelope field $\underline{E}(x,t)$ in this case can be modeled by a sum over events i:

$$\underline{E}(x,t) = \sum_{i=0}^{N(t)} \underline{\hat{\epsilon}}_i(\underline{x} - \underline{x}_i, t - t_i) + \underline{E}_{nonlocal}(\underline{x},t) \qquad (3.1)$$

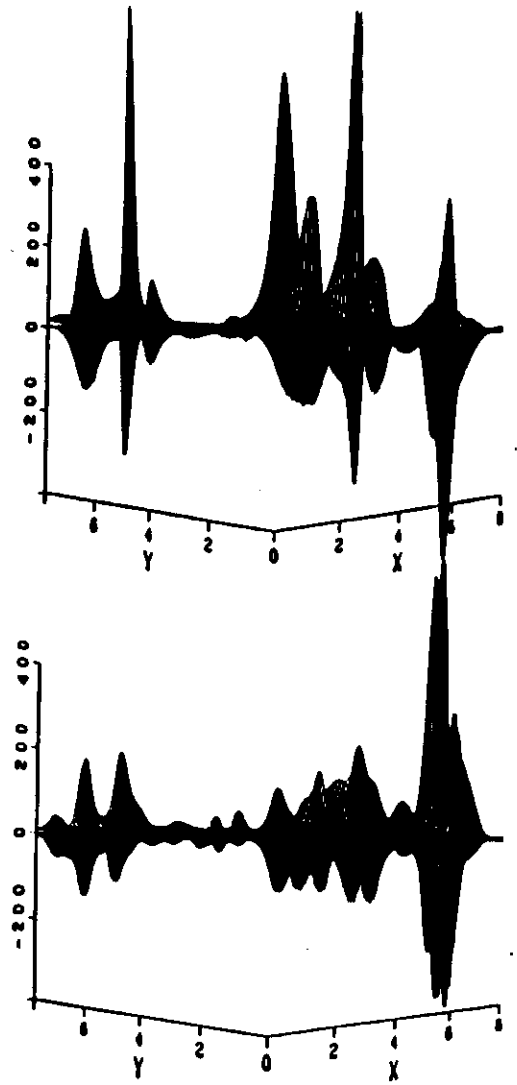

Fig. 1

Two-dimensional plots of $|E|^2$ (upper surface) and n (lower surface) at two different times. Parameters in scaled units $E_0 = 1.2$, $\nu_i = 0.9$, $\omega_c/\omega_p = 0$, ν_e = Landau damping continued smoothly as k^2 at large k, $m_i/\eta m_e = 1836$, $L_x = L_y = 2\pi$ and a 128 x 128 spatial grid. The collapses are anisotropic with the narrow dimension along the x axis, the drive direction

Here a caviton event i is localized at the space time point $\underline{x}_i$, t_i. The single event function $\underline{\xi}_i(\underline{x},t)$ has its maximum at x=0, t=0 with a spatial width $\delta_i(t)$ and a temporal width or lifetime τ_i; from the simulations we find this lifetime to be or the order of 0.05 to 0.1 ms for ionospheric parameters. At a given time t, the number of events N(t) which contribute to the sum in (3.1) are those for which $0<t-t_i<\tau_c$ which is clearly proportional to the volume of the system if the cavitons are roughly uniformly distributed. For example, if the portion of the heated volume observed by the radar is ionospheric heating experiments is $(200\ m)^3$, the mean caviton spacing is 0.25 m which is about 50 λ_{De} as observed in our simulations, and the mean time between events is roughly τ_c as observed in our simulations, then we find $N(t) \sim 10^7$ which is crude but representative. In (3.1) the term $\underline{E}_{nonlocal}(\underline{x},t)$ represents the nonlocalized part of the envelope field which we will assume is relatively negligible.

This local caviton model can be put into a more formal setting by introducing the instantaneous vector eigenfunctions $\underline{\varepsilon}_\nu(\underline{x},t)$ of the operator on the left hand side of (2.9a). These satisfy (for $B_0 = 0$)

$$\underline{\nabla} \cdot \left[\lambda_\nu(t) + \nabla^2 - n(\underline{x},t)\right] \underline{\varepsilon}_\nu(\underline{x},t) = 0 \tag{3.2}$$

where $\lambda_\nu(t)$ is the corresponding instantaneous eigenvalue and $\underline{\nabla} \times \underline{\varepsilon}_\nu = 0$. These are nothing more than the Langmuir modes in a nonuniform density background. In ordinary units this can be written as

$$\underline{\nabla} \cdot \left[\omega_\nu - \omega_p(x,t) + \frac{3}{2}\lambda_D^2 \omega_{Po} \nabla^2\right] \underline{\varepsilon}_\nu(\underline{x},t) = 0 \tag{3.3}$$

where

$$\omega_p(x,t) = \omega_{P_0}\left(1 + \frac{1}{2}\frac{n(xt)}{n_0}\right)$$

is the spatially fluctuating plasma frequency. Thus we can relate λ_ν in scaled units to ω_ν in ordinary units:

$$\lambda_\nu(t) = \frac{\omega_\nu - \omega_{P_0}}{\omega_{P_0}} \cdot \frac{2}{3}\left(\frac{m_i}{\eta m_e}\right)^{1/2} \tag{3.4}$$

The complete description of these states for an arbitrary $n(\underline{x},t)$, especially for $D \geq 2$ is beyond our capability. In D = 1 it is relatively easy to compute these states from

an arbitrary realization of n(x,t) obtained from the complete numerical simulation of (2.9a,b).[6] We note that a subset {i} of the states {ν} are localized at $x=x_i$ in density depressions of $n(\underline{x},t)$ and some of these, which have the proper symmetry to couple to the pump $\underline{E}_0$, evolve to collapse. This subset of states can be viewed as local ground states of the "potential" $n(\underline{x},t)$.

The electric field envelope can be resolved in this complete set of states

$$\underline{E}(x,t) = \sum_\nu h_\nu(t)\underline{\varepsilon}_\nu(\underline{x},t)exp(-i\omega_0 t) \tag{3.6}$$

(In an infinite system the sum may imply an integral over continuum states.) The equation of motion for the amplitudes $h_\nu(t)$ is readily found from (2.9a) to be

$$i\dot{h}_\nu(t) + (\omega_0 - \lambda_\nu(t)h_\nu(t) + i\sum_{\nu\prime}\left[(\underline{\varepsilon}_\nu \phi \nu_e \underline{\varepsilon}_{\nu\prime}) + (\underline{\varepsilon}_\nu \phi \dot{\underline{\varepsilon}}_{\nu\prime})\right] h_{\nu\prime} = \underline{E}_0 \cdot (\underline{\varepsilon}_\nu|n) \tag{3.7}$$

Here we have taken the $\underline{\varepsilon}_\nu$ to be a complete orthonormal set with

$$(\underline{\varepsilon}_\nu \phi \underline{\varepsilon}_{\nu\prime}) = \int d\underline{x}\,\underline{\varepsilon}^*_\nu(\underline{x},t) \cdot \underline{\varepsilon}_{\nu\prime}(\underline{x},t) = \delta_{\nu\nu\prime} \tag{3.8}$$

and have used the notation

$$(\underline{\varepsilon}_\nu \phi \dot{\underline{\varepsilon}}_{\nu\prime}) = \int d\underline{x}\,\underline{\varepsilon}^*_\nu(\underline{x},t) \cdot \frac{d}{dt}\underline{\varepsilon}_{\nu\prime}(\underline{x},t) \tag{3.9a}$$

$$(\underline{\varepsilon}_\nu \phi \nu_e \underline{\varepsilon}_{\nu\prime}) = \int d\underline{x} \int d\underline{x}'\underline{\varepsilon}_\nu(\underline{x},t) \cdot \nu_e(\underline{x}-\underline{x}')\underline{\varepsilon}_{\nu\prime}(\underline{x}',t) \tag{3.9b}$$

$$\underline{E}_0 \cdot (\underline{\varepsilon}_\nu|n) = \underline{E}_0 \cdot \int d\underline{x}\,\underline{\varepsilon}^*_\nu(\underline{x},t)n(\underline{x},t) \equiv S_0 \tag{3.9c}$$

To understand the various terms in (3.7) first consider the case where $n(\underline{x})$ is independent of time and therefore $(d/dt)\,\underline{\varepsilon}_\nu(\underline{x}) = 0$. Then the amplitude h_ν is driven directly by the source term $\underline{E}_0 \cdot (\underline{\varepsilon}_\nu|n)$. If $\underline{\varepsilon}_\nu$ where a plane wave state proportional to exp i $\underline{k}\cdot\underline{x}$; then this source term is proportional to $\underline{E}_0 \cdot \underline{k}\, n(\underline{k})$ the so called direct conversion source term.[12,1] However, the important states are the localized states. The coefficient $(\underline{\varepsilon}_\nu \phi \nu_e \underline{\varepsilon}_{\nu\prime})$ couples states because of the nonlocal nature of the

Landau damping. This term becomes important in the time dependent case only in the burnout phase. Note that by introducing the spatial Fourier transform of the eigenstates $\underline{e}_\nu(k,t)$ we can write

$$(\underline{e}_\nu \phi \nu_e \underline{e}_{\nu'}) = \sum_{\underline{k}} \underline{e}^*_\nu(\underline{k},t) \cdot \underline{e}_{\nu'}(\underline{k},t)\nu_e(\underline{k}) \tag{3.10}$$

For $\nu=\nu'$ this certainly becomes important in the burnout phase. For $\nu \neq \nu'$ this is less important if one of the states is not localized - e.g., noncollapsing - or is localized at a different space-time point.

In the time-dependent case of interest the coefficient $(e_\nu \phi \dot{e}_{\nu'})$ can provide a coupling between rapidly collapsing states, say ν' and a nonlocalized state ν. This is one of the mechanisms responsible for the excitation of the "free mode" states observed in the spectra. We will return to this in more detail below.

We can now make a tentative connection between the localized event functions $\hat{\underline{\varepsilon}}_i\,(x - x_i, t - t_i)$ of (3.1) and the subset $\{i\}$ of localized eigenstates. It is reasonable to identify

$$\hat{\underline{\varepsilon}}_i(\underline{x} - \underline{x}_i, t - t_i) = \underline{e}_i(\underline{x} - \underline{x}_i, t - t_i)exp(-i\omega_0 t) \tag{3.11a}$$

where

$$\underline{e}_i(\underline{x} - x_i, t - t_i) = h_i(t)\underline{e}_i(\underline{x}, t) \tag{3.11b}$$

The contributions from the remaining nonlocalized states in the set $\{\nu\}$ make up the term $\underline{E}_{nonlocal}\,(x,t)$ in (3.1).

The eigenstates $\underline{e}_i(\underline{x},t)$ are in a sense the natural basis or coordinates for describing the turbulent system. Unfortunately, they can only be obtained by first solving (2.9) for $n(\underline{x},t)$. In spite of this they are conceptually useful and some observed properties of the turbulence can be related to general properties of these states. In effect the use of the states $\underline{e}_i(\underline{x},t)$ represents a huge reduction in the effective dimensionality of the problem. While we use $(128)^2$ Fourier modes for the simulation there may be of the order of 10 collapse sites in the cell and therefore roughly 10 localized states.

We have gained useful insight into the nature of these eigenstates and their connection to the observed turbulence by considering the scalar Zakharov model. In this model $E(r,t)$ and E_0 are scalar fields and in place of (2.9) we have

$$\left[i(\partial_t + \nu_e\bullet) + \nabla^2 - n(\underline{x},t)\right] E(\underline{x},t) = E_0 n(\underline{x},t) \tag{3.12a}$$

$$(\partial_t^2 + 2\nu_i\bullet\partial_t - \nabla^2)n(\underline{x},t) = \nabla^2|E_0 + E(\underline{x},t)| \tag{3.12b}$$

In this model only spherically symmetric collapsing cavitons are allowed and the three dimensional problem for an isolated collapse reduces to one in which E and n depend only on the radial coordinate r. This scalar model has several properties in common with the physical three-dimensional vector model (2.9): threshold and maximum growth rate for the modulational instability, collapse scaling exponents which are discussed below, no threshold energy for collapse and the possible failure of a density well to support a localized eigenstate.

Spherical symmetry is imposed by representing all fields in terms of the Fourier modes $\sin(k_\ell r)$, $k_\ell = \pi\ell/r_0$, $\ell = 1,2,--$, with r_o chosen large compared to a typical caviton size. In these scalar studies we have observed for $\nu_i(k)/k = 0.9$ that at the nucleation site, $E(r,t)$ is dominated by its projection, $h_0(t)$, on the localized ground state $e_0(r,t)$. In nucleation $e_0(r,t)$ remains localized; at every time step $e_0(r,t)$ can be computed from $n(r,t)$. Here we will adopt a simplified model in which $h_0(t)$ is evolved neglecting the excited state contributions $\nu' \neq 0$ in (3.7). The density evolves according to (3.12b) with the pondermotive force replaced by $\nabla^2|E_0 + h_0(t)e_0(r,t)|^2$. The solution to this model is insensitive to boundary conditions (i.e., the choice of r_0).

Let us restrict our attention to the case where ν_i is large enough so that after burnout, the relaxing density fluctuation is essentially nonpropagating. Immediately after burnout, energy absorption is minimal because the eigenvalue is large and negative, implying a far from resonant coupling to S_0 (see (3.9c)). The pondermotive force is negligible, and the density fluctuation evolves according to the acoustic Green's function. A simple model for this phase of the dynamics is obtained by replacing the rhs of (3.12b) by $I\delta(t)\,\nabla^2\delta^3(\underline{x})$, where the "impulse" $I \equiv \int dt \int d\underline{x}|e(\underline{x},t)|^2 = \int |h_0(t)|^2\,dt \approx (|h_0|^2)\tau$. In three dimensions, the response of n is

$$n(x,t) = I \cdot G(|x|/t)/t^4 \qquad (3.13a)$$

where

$$G(\rho) = \frac{\nu_i}{\pi^2 \rho} \frac{d^2}{d\rho^2} \left[\frac{\rho}{(1+\rho)^2 - 4\rho^2(1-\nu_i^2)} \right] . \qquad (3.13b)$$

Even though n is evolving self similarly, $\underline{e}_0$ is not. The figure of merit, μ, for the ground state is simply expressed in terms of the width w, $w(t) \sim t$, of n, and its depth, d, $d \sim I/t^4$, as $\mu \sim dw^2 \sim I/t^2$. If μ is too small, there is no localized state. Since 3D solitons are unstable, as t increases, either enough energy will be accumulated so that another collapse follows, or the bound state will be lost. In the latter case, the bound state will be localized in the immediate vicinity of the expanding-density fluctuation, until just before the bound state is lost. So that during the time when energy is being injected, one may be able to ignore the coupling between states localized at different collapse sites. At a particular collapse site there is a lowest lying localized state which has a nonzero source. Excited states at the same site typically have a smaller source term because they are oscillatory while $\underline{E}_0$ $n(\underline{x},t)$ is essentially uniform in direction. Also at a particular site there may only be a small number of localized states. This motivates the study of a model for the evolution of a caviton in a previously existing density fluctuation - a process we call caviton nucleation - in which only one localized state is present. For a given ion fluctuation the lowest lying state, $\underline{e}_0$, with nonvanishing source, S_0, (we shall call it the ground state) is calculated from (3.9c), h_0 is evolved according to (3.7) without the coupling to other amplitudes.

In Figure 2 we show some typical results from the scalar model driven by a spatially uniform field E_0 at the plasma frequency ($\omega_0 = 0$). For a range of E_0, a stable nucleation cycle is observed, with a complete cycle over the interval $0<t<t_c$. We expect that in a turbulent environment of other such nucleation sites, the strict periodicity of this cycle may be lost, but at a given site there may be strong correlations over a few cycle times for strong ion acoustic damping.

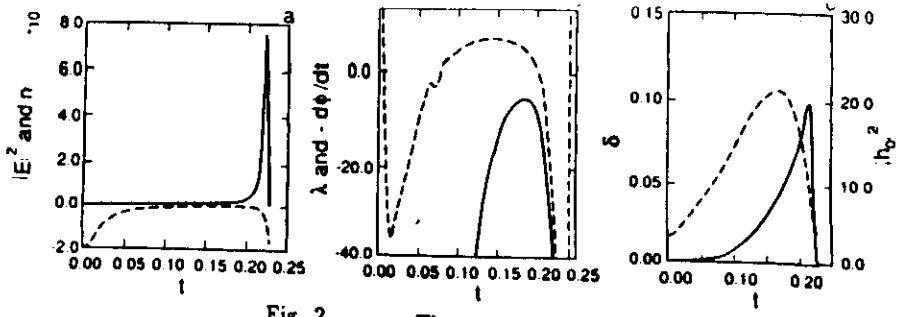

Fig. 2 **The temporal evolution of (a) $|E(r=0,t)|^2$ and $n(r=0,t)$, (b) $\lambda_0(t)$ and the phase velocity $-d\phi/dt$ and (c) the caviton width $\delta(t)$ and the electrostatic energy in the caviton $|h_0(t)|^2$.**

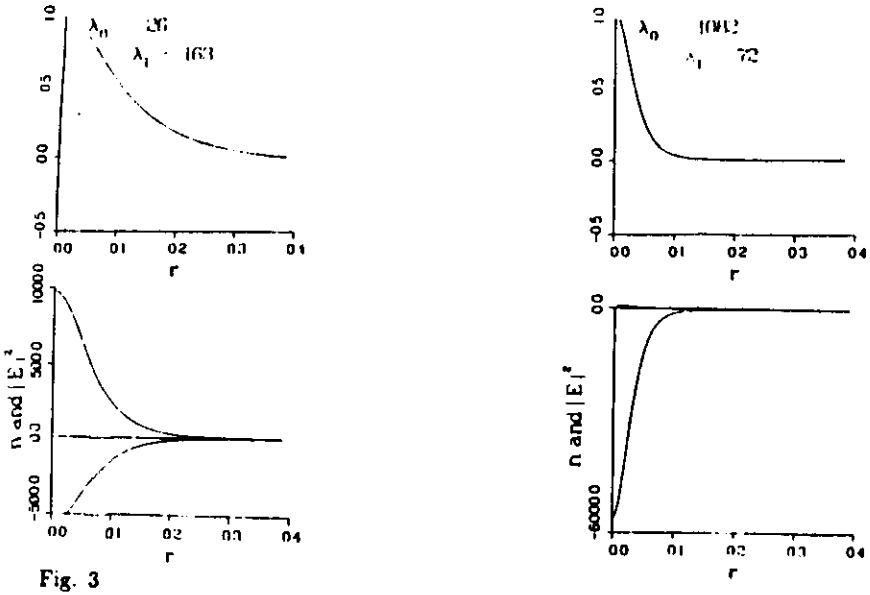

Fig. 3

Scalar model for $E_0 = 1.8$, $m_i/m_e = 2\times10^{-4}$, $\nu_i = 0.9$, $\omega_0 = -80$. Showing shape of $n(r,t)$ and $|E(r,t)|^2$ as functions of r for two times in the caviton cycle evolution and the profiles of the two lowest eigenfunctions $e_0(r,t)$ and $e_1(r,t)$ vs r at the same times. The qualitative behavior is the same for the case $\omega_0 = 0$.

In Figure 3 we show snapshots of the lowest two eigenstates $e_0(r,t)$ and $e_1(r,t)$ and the density $n(r,t)$ as they evolve during one of these cycles for a case where $\omega_0 < 0$. In Figure 2a we show the time evolution of $|E(r = 0,t)|^2$ and $n(r=0,t)$, in Figure 2b the ground state eigenvalue $\lambda_0(t)$, the velocity Φ_0 of the phase of the amplitude $h_0(t) = |h_0(t)| \exp i\Phi_0(t)$, and in Figure 2c the electrostatic energy in the caviton $|h_o(t)|^2$. At the beginning of the cycle, t=0, the deep density well is relaxing from the previous burnout. From Fig. 2a we see that the peak $|E|^2$ occurs at about t=0.22 followed by its rapid burnout due to dissipation. The density well reaches its maximum depth shortly after at $t \simeq 0.235$. The maximum spatial extent of the eigenfunction $\delta(t)$ occurs earlier at $t \simeq 0.15$ which is also the time at which the well depth, $n(r=0,t)$, is shallowest. The well then deepens under the action of the PMF increasing the confinement of the eigenfunction. The eigenvalue $\lambda_o(t)$ approaches the pump frequency $\omega_0 = 0$, this causes a rapid increase in $|h_0(t)|^2$ as the mode frequency approaches resonance with the pump frequency. This rapidly increases the PMF and as the density well deepens again $\lambda_0(t)$ again decreases rapidly during collapse. This illustrates what we believe to be the typical behavior: As the relaxing density well becomes shallower and broader its eigenvalue approaches resonance with the pump causing a rapidly increasing PMF which initiates the next collapse. It is, of course, important that the state remain localized so that it maintains a significant PMF. Under some conditions for $D \geq 2$ a localized bound state can be lost, i.e., λ_0 crosses zero before sufficient PMF is built up to initiate collapse. For the D=3 scalar model discussed here we find a finite nucleation threshold [Rose et al. 1986]. For E_0 below this value the cycle cannot be maintained.

There are certain qualitative features of the scalar model which enable one to make scaling predictions. This has been discussed by Rose et al.[11] Consider a regime in which E_0 is time independent, and dissipative effects are significant during a time very short compared to τ, the caviton cycle time, with the cycle beginning at t=0, and ending at $t=\tau$. We shall call this ideal nucleation. One dimensionless parameter of nucleation is the degree of localization, μ, at the turnaround time, t_1, when δ begins to shrink. This can also be expressed in terms of the impulse I, (3.13a), which drives the density well: $\mu = I/t^2$ where t is the time elapsing since the previous collapse. For $0<t<t_1$, the pondermotive force is negligible, and one obtains the estimates $\delta(t=t_1) \equiv \Delta \sim t_1$. and $\mu \sim I/{t_1}^2$. Near turn-around, $|\lambda_0|$ attains its smallest value, Λ, (for an isolated nucleation site, localization requires $\lambda_0 < 0$), and $|h_0|^2$ attains its maximum value, N_{max}. If one makes the hypothesis,

justified by the results of Figure 5a, that μ does not depend sensitively on E_0, then $\Lambda \sim 1/\Delta^2$. We now distinguish two regimes: $(\tau - t_1)\,\Lambda < 1$, and $(\tau - t_1)\,\Lambda >> 1$. The former will be called sonic nucleation, and the latter supersonic nucleation.

The sonic regime is obtained for $E_0 \approx E_T$ where E_T is the threshold value of E_0, above which stable caviton cycles are obtained. At turn-around, the cavity is closest to resonance, and the oscillations in $|h_0|^2$ are potentially large. However, there is not sufficient time between turn-around and burnout for these large oscillations to take place, so that $N_{max} \approx N(\tau)$, the amount of energy taken into burnout, which is also the amount of energy dissipated, D. In this regime, one finds that $(\tau - t_1)/\tau << 1$, and therefore

$$\mu \sim I/\tau^2, I \sim N_{max}\,\tau, \Delta \sim \tau \tag{3.14}$$

The evolution of the caviton parameters for $E_0 = 3.40$, and no damping until the very end of the cycle, are shown in Figure 4. Note that the major variation in time of $|h_0|^2$ is on the time same τ, which may be reinterpreted as the sonic transit time over Δ, and that is why we call this sonic nucleation. Relations (3.14) do not depend explicitly on E_0, and so we shall call them internal scaling relations. If one assumes that collapse sites are typically situated a distance Δ from each other, then the mean energy density $(|E|^2) \equiv W \sim N_{max}/\Delta^3 \sim 1/\Delta^2$, and the mean dissipation rate (per unit time per unit volume) $R \sim W/\tau \sim 1/\Delta^3$. Therefore

$$R \sim W^{3/2}\,. \tag{3.15}$$

Note that (3.15) is identical to the result obtained by Degtyarev et al. [1984] by using an analysis based on the modulational instability.

Another set of scaling results is obtained by relating the above quantities, i.e., N_{max} and Δ, to E_0. From dimensional analysis the source term in (3.9c) can be estimated as $E_0\lambda_0\delta^{3/2}$. The maximum amplitude $|h_0|$ is then simply estimated as $E_0\Delta^{3/2}$, because the oscillation amplitude of a nonresonantly driven oscillator $\sim$ (source/frequency mismatch). Therefore

$$N_{max} \sim E_0^2\Delta^3\,. \tag{3.16}$$

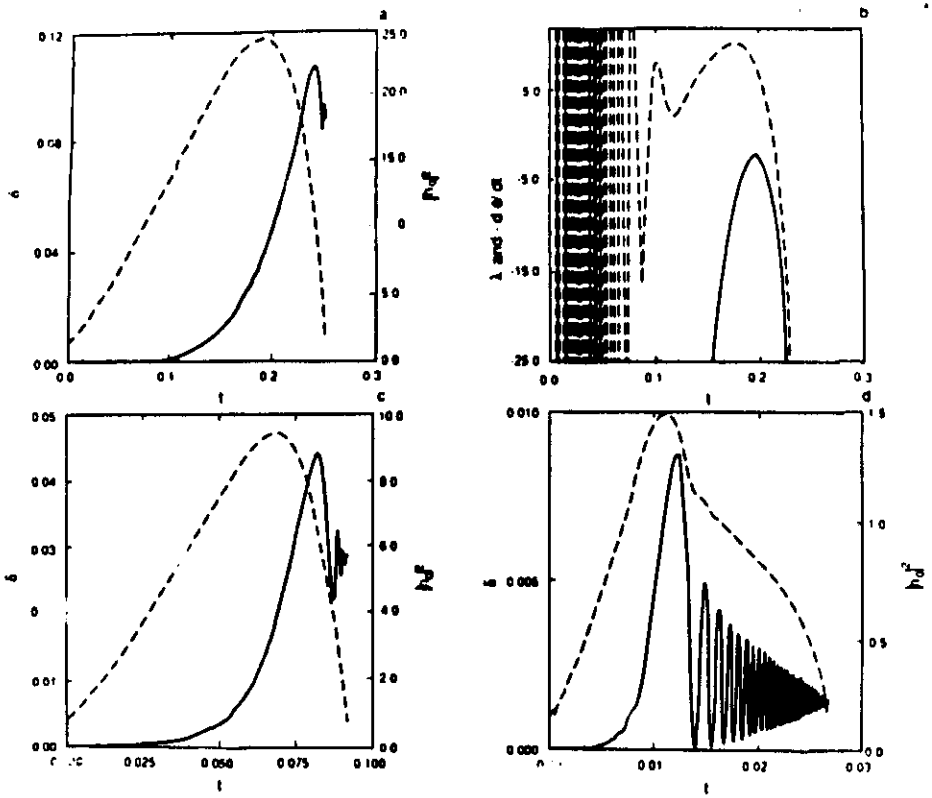

Fig. 4

Evolution of the ground state radius δ and the electrostatic energy

for the parameters of

Fig. 2. but with no dissipation. (a) and (b) $E_0 = 3.4$, and (c) $E_0 = 8.0$, and (d) $E_0 = 32.0$.

Combining (3.14) and (3.16) one obtains

$$W \sim E_0^2, R \sim E_0^3, N_{max} \sim 1/E_0, \Delta \sim \tau \sim 1/E_0, \Lambda^{-1} \sim 1/E_0^2 \sim I\,. \qquad (3.17)$$

In words, the stronger the drive, the weaker, smaller, and briefer are individual collapses, in a way such that the overall dissipation rate is greater. As far as we can tell, the results in (3.17) are quite different from those predicted from a modulational instability analysis.

As E_0 increases, $(\tau - t_1)\,\Lambda$ becomes large and we encounter the supersonic nucleation regime, there are large oscillations in N for $t_1 < t < \tau$, and D decreases faster than N_{max}. The evolution of N for $E_0 = 8.0$ and 32.0 is shown in Figure 4. In Figure 5 variations of μ, N_{max}, D, Δ, τ, and Λ are shown for $3.4 < E_0 < 32.0$. Towards the end of this range, $D\,E_0^2 \approx$ constant. The ansatz that the figure of merit, μ, is constant is not too badly violated away from the nucleation threshold, and the measured scaling exponents are close to the values in (3.17). An eyeball fit (the dashed lines in Fig. 5) yields $N_{max} \sim 1/E_0^{5/4}$, $\Delta \sim 1/E_0^{7/6}$, $\tau \sim 1/E_0, \Lambda \sim E_0^2$. The scaling of R is roughly $R \sim E_0^2$.

In order to physically realize ideal nucleation, dissipative effects must be negligible when energy is being absorbed. Peak absorption rate occurs roughly at the same time that the caviton is fattest with width Δ. In dimensionless units the Debye wavenumber $\sim [M \equiv m_i/\eta m_e]^{1/2}$. Therefore, if $\Delta M^{1/2} \sim M^{1/2} / E_0^{7/6} >> 1$, nucleation will be essentially nondissipative. Ignoring the difference between 7/6 and 1, and recalling the units of electric field strength, this means the energy density of the external field must be small compared to the particle kinetic energy density.

For example, if $E_0 = 8.0$, numerical studies indicate that $M > 40{,}000$, i.e., field energy/kinetic energy < 0.003, is required in order that D be within 20% of the ideal value. This estimate of a few tenths of one percent does not depend sensitively on M.

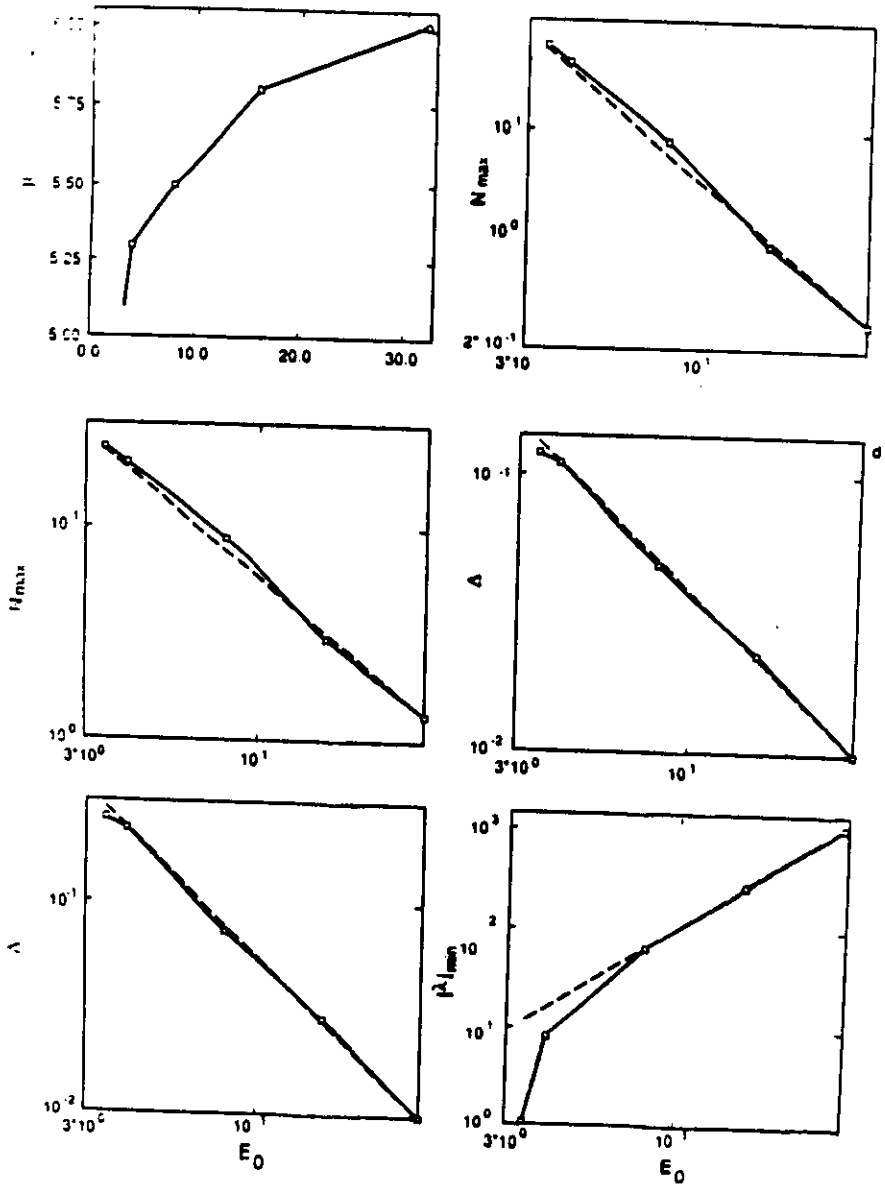

Fig. 5 Scaling behavior in scalar model. (a) μ, (b) N_{max}, (c) dissipation (energy dissipated at end of collapse), (d) nominal width of caviton ground state, Δ, (e) caviton cycle period τ, and (f) minimal |λ| all vs E_0.

In this regime ($\bar{E}_0^2/4\pi n_0 T_e$ <1) the scaling $DE_0^2 \sim$ const. has an interesting consequence if it is assumed that the scale of the caviton δ(diss) at the end of collapse, i.e. at the beginning of dissipation is independent of E_0 (say 5 λ_{De} in physical units). Then since D is the energy dissipated at the end of collapse we have $D \sim |E|^2_{peak}\, \delta^3(diss) \sim$ const. E_0^{-2} so $|E|^2_{peak} \sim E_0^{-2}$; the peak field in the caviton actually decreases with increasing driving strength!

For fixed *physical value* of the electric field, if M is quadrupled, E_0 doubles, Δ and τ are approximately halved, *physical* length scales are roughly invariant while the *physical* caviton cycle time doubles. Any fixed *physical frequency*, such as the electron-ion collision rate, or frequency mismatch between the external electric field and the average plasma frequency, becomes more important as M increases.

This isolated collapse model is oversimplified in several ways, one is its neglect of the turbulent environment of the collapse site. The density fluctuation n(r,t) was constrained so that there was locally no net change in particle number - i.e., $\int d\mathbf{r}\, r^2(r,t)=0$ - i.e., the local averaged plasma frequency is the same as the global average plasma frequency which is the zero of frequency in our envelope approximation. This constrains all bound or localized states to have $\lambda_\nu(t)<0$. However, locally on a scale larger than a single caviton but macroscopically small there can be fluctuations in the background plasma frequency away from the global average. If the local plasma frequency is different from zero this is equivalent to replacing n(r,t) in (5.12a) by δn_0 + n(r,t) and bound states can occur if $\lambda_\nu < \delta n_0$. Since there are local domains or "patches" of positive and negative δn_0 we conclude that in a large multicaviton system localized states can occur for $\lambda_\nu(t)<(\delta n_0)_{max}$ where $(\delta n_0)_{max} >0$ and depends on the parameters E_0, ω_0, etc. which determine the turbulent state. Simulations with $\omega_0 >0$ are consistent with this picture. The "localized" states for $\delta n_0 >0$ are not strictly localized from the mathematical point of view; their eigenfunctions may have extended tails which are exponentially small but do not decay at large distances. Such states are better described as resonance states as discussed at the end of this section.

The self similar scaling of the parameters of the eigenstates during the collapse phase are well-known [e.g., Galeev et al.[9]]. A self-similar ansatz for $\underline{\varepsilon}_i(\underline{x},t)$ can be written

$$\underline{e}_i(\underline{x},t) = \frac{1}{\delta^{D/2}(t)}\,\hat{\underline{e}}(\underline{x}\delta^{-1}(t) \qquad (3.18a)$$

where $\hat{e}(\zeta)$ is the normalized shape function of the collapsing state.

$$\int d\zeta|\hat{e}(\zeta)|^2 = 1 \qquad (3.18b)$$

The collapses observed in our D = 2 simulations are not cylindrically symmetric as can be seen in Figure (4.2), but have a pancake shape with the narrow direction mainly aligned along the pump polarization (the x direction in Figure 1). The aspect ratio of the y dimension to the x dimensions appears to be in the range of 2 to 3. The ansatz of (3.18) implies that although the aspect ratio is not necessarily unity all dimensions scale with $\delta(t)$. Simulations of collapse in D = 3 for isolated cavitons[27] and for multicaviton states[5] display these pancake cavitons whose orientation arises either as a result of initial conditions or by coupling to a drive source such as we have used.

The scaling of the parameters of the self-similar collapse depend on the spatial dimension D as follows:

$$\delta(t) = (t_c - t)^{2/D} \qquad (3.19)$$

$$\lambda(t) \sim \delta^{-2}(t) \sim (t_c - t)^{-4/D} \qquad (3.20)$$

where t_c is the time of collapse. The self-consistent density behaves as

$$n(\underline{x},t) = -\frac{1}{\delta^2(t)}\,G(\underline{x}\delta^{-1}(t)) \qquad (3.21)$$

where $G(\underline{x}\delta^{-1}(t))$ is a shape function related self-consistently to $\hat{e}(\underline{x}\delta^{-1}(t))$. The scalar model collapse behavior is consistent with these scalings for D = 3.

We will use the self-similar formula (3.18) for $\underline{e}_i(\underline{x},t)$ in other regimes -- e.g., nucleation but where $\delta(t)$ does not satisfy the scaling of (3.19). Examples of the evolution of $\delta(t)$ in the scalar model are shown in Figure 4.

In the scalar model results, presented above, the contributions from nonlocalized states or from localized excited states are neglected. Such localized excited

eigenfunctions have one or more nodes in the region of the confining density well and would be expected to couple less efficiently to the pump in the overlap integral of (5.9c). Localized excited states which evolve to collapse are not observed in the simulations.

For an isolated density well the localized state eigenfrequencies lie below those of the nonlocal (or continuum) states. In the "patchy" model with fluctuating domains of differing mean plasma frequency, it appears that the eigenvalue ranges of localized and nonlocalized states may overlap.

The definition of a localized state as one of the localized eigenfunctions $\underline{e}_i(\underline{x},t)$ is actually too restrictive. A wavepacket of nonlocalized states whose λ_ν lie just above the localization limit can be a resonance state analogous to those known in quantum mechanical scattering theory if it is a superposition of states with a sharp peak in the density of states. Such a resonance state will appear spatially coherent and localized for a time $\Delta t \sim (\Delta\lambda)^{-1}$ where $\Delta\lambda$ is the frequency width of the resonance. The resonance state will then have a pondermotive force over a time which may be sufficiently long to depress the density so that a strictly localized eigenstate can again appear. The effective source terms $E_0 \bullet (e_\nu n)$ are nearly the same for all the states comprising the resonance. A narrow resonance state therefore cannot be distinguished from a strictly localized eigenstate and so the definition of the states $\underline{e}_i(x,t)$ which are identified in (3.11) should be extended to include such narrow resonance states. It can be shown that for a sufficiently narrow resonance the equation of motion for its amplitude $h_i(t)$ is indistinguishable from the equation of motion discussed above for a localized state. The existence of such resonances is another reason why localized states appear to exist for $\lambda_i > 0$. As discussed above, the random density environment of a caviton can also raise the eigenvalue limit for localization to positive values. Such localized states are also best described as resonance states.

4. ENERGY SPECTRA AND POWER SPECTRA IN THE LOCAL CAVITON MODEL

It is well-known that the power spectrum of electron density fluctuation, $\tilde{n}_e(\underline{x},t)$, contains information concerning the elementary excitations of a plasma and can be measured by incoherent Thomson scatter techniques. For frequencies ω near the

electron plasma frequency ω_p (or its negative) the ions cannot respond significantly and so one can relate the electron density fluctuation directly to the total electric field

$$4\pi e\,\tilde{n}_e(\tilde{x},t) = \nabla\cdot\tilde{E}_{TOT}(\tilde{x},t) \;=\; \frac{1}{2}\nabla\cdot\tilde{E}(\tilde{x},t)e^{-i\omega_p t} \;+\; c.c. \qquad (4.1)$$

From this it is easy to see that the power spectrum of n_e is directly related to that of the envelope field

$$\begin{aligned}(4\pi e)^2|\tilde{n}_e(\underline{\tilde{k}},\omega)|^2 &= (1/4)|\underline{\tilde{k}}\cdot\;\underline{\tilde{E}}(\underline{\tilde{k}},\tilde{\omega}-\omega_p)|^2\\ &= (1/4)(\tilde{k}\lambda_D)^2\underline{\tilde{E}}(\underline{\tilde{k}},\tilde{\omega}-\omega_p)|^2(4\pi n_0 T_e)^{-1}\end{aligned} \qquad (4.2)$$

To obtain the low-frequency spectrum associated with the ion line we note that for $\omega << kv_e$ that quasineutrality is obtained so $n_e(\tilde{k}\,\tilde{\omega}) \simeq n_i(\tilde{k},\tilde{\omega}) = n(\tilde{k},\tilde{\omega})$ and the low frequency electron density spectrum is obtained directly from the density fluctuation which appears in the Zakharov model:

$$|\tilde{n}_e(\underline{\tilde{k}},\tilde{\omega}|^2 = |\tilde{n}(\underline{\tilde{k}},\tilde{\omega})|^2 \qquad (4.3)$$

The power spectra can be found by taking the temporal Fourier transform of (3.1).

$$\underline{E}(\underline{k},\omega)_T \;=\; \sum_i^{N(T)}\; exp i[\underline{k}\cdot\underline{x}_i - \omega t_i]\underline{\varepsilon}_i(\underline{k},\omega)_t + \underline{E}(k,\omega)_{nonlocal} \qquad (4.4a)$$

where

$$\underline{\varepsilon}_i(\underline{k},\omega)_t \;=\; \int_{t-T/2}^{t+T/2} dt'(t'-t_i)\underline{\varepsilon}_i(\underline{k},t'-t_i)\; exp[i\omega(t'-t_i)] \qquad (4.4b)$$

is the single event Fourier coefficient. If we make the assumption, which is probably invalid, that all events are uncorrelated we obtain the power spectrum as a sum over single event spectra:

$$\langle|\underline{E}(\underline{k},\omega_t|^2\rangle \;=\; \sum_{i=1}^{N(T)}|\underline{\varepsilon}_i(\underline{k},\omega)|^2 \;\equiv\; N(T)\langle|\underline{\varepsilon}(\underline{k},\omega)|^2\rangle \qquad (4.5)$$

The important effect of correlations will be discussed below.

Simulation parameters can be chosen so that the collapse events are so well separated in time that we were able to compute the single event spectra $|\underline{\varepsilon}\;(\underline{k},\omega)|^2$ for this case. These spectra, shown in Figure 6, have a surprisingly rich structure including the following features: 1.) Essentially all the spectra energy occurs for $\omega < \omega_0$; in this case $\omega_0 = 0$; 2.) There are well defined peaks in the spectrum; 3.) For increasing k, i.e., increasing $k\lambda_D$, the peaks for more negative ω become relatively more important; 4.) The position of the maximum shifts in a step-wise fashion (see inset to Figure 6) where $-\omega_{max} \sim k$, i.e., $\omega_p - \tilde{\omega}_{max} \sim \tilde{k}\,c_S$; 5.) There is a weak "free mode" peak at $\omega \sim k^2$, i.e., roughly at the Bohm-Gross frequency. These single event spectral properties are similar to those shown in Figure 8 for the power spectra from multicaviton states in a magnetic field.[1] Caviton-caviton correlations also can have a strong effect on the spectral shape and will be discussed below.

We have obtained some insight into the sources of this structure from the scalar model discussed in Sec. 3. A realization of the single event spectrum $|\varepsilon\;(\underline{k},\omega)|^2$ for the scalar model is constructed by taking the temporal transform of the function $f(t) = h_0(t)e_0(k,t)$ for $0<t<\tau_c$ and $f(t) = 0$ for $\tau_c < t < T$ where T is chosen to give the desired frequency resolution and $e_0(k,t)$ is the spatial Fourier transform of the numerically obtained $e_0(r,t)$. The results are shown in Figure 7. These model spectra contain the features listed above for the D = 2 Zakharov model (Fig. 6) except for 4.) and 5.).

The predominance of negative frequencies arises because the phase velocity $\dot{\Phi}$ is in Figure 4 is predominantly negative; this in turn is related to the negativity of the eigenvalue $\lambda(t)$. In this model calculation Eq. 3.7 reduces to $i\dot{h}_0 - \lambda_0 h_0 = S \equiv E_0\langle e_0|n\rangle$ since we are neglecting coupling to excited states. Then if we write $h_0 = |h_0|\exp i\Phi_0$ we see that $\dot{\Phi}_0$ is related to λ_0 by

$$-\dot{\Phi}_0 = \lambda_0(t) + S(t)|h_0|^{-1}cos\Phi_0 \qquad (4.6)$$

which is the equation used to compute Φ_0 in Figure 4.

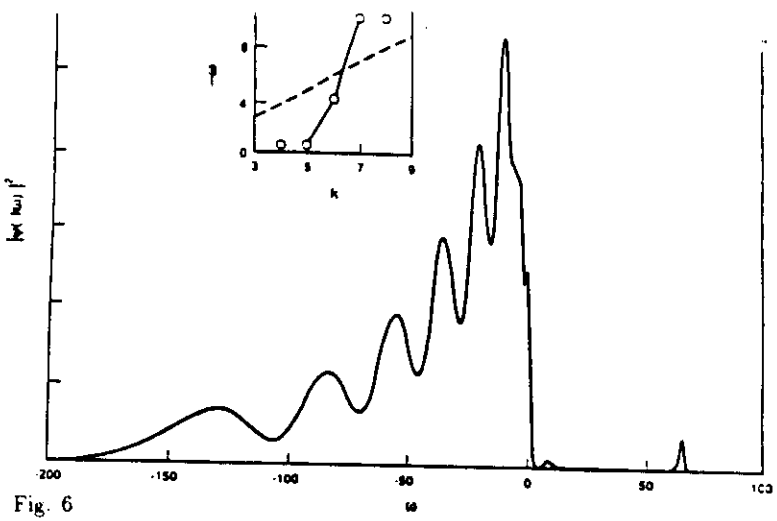

Fig. 6

Spectra, $|\psi(\underline{k},\omega)|^2 = k^{-2}|E(\underline{k},\omega)|^2$, for D=2 isolated collapse events. $E_0=0.8$, $v_i=0.9$, $m_i/m_e=1836$, $\omega_0=0$. $k_x=8$, $k_y=0$

. Inset Solid line, negative frequency at maximum of spectrum vs $k=k_x$; dashed line, ion acoustic frequency shift, $|\omega|=k$.

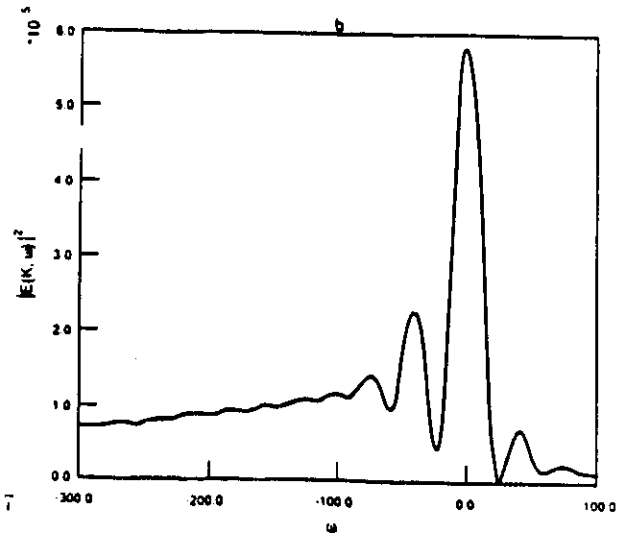

Fig. 7

Power spectra $|E(\underline{k},\omega)|^2$ for the scalar model parameters of Fig. 2.

Spectrum for k = 40.0.

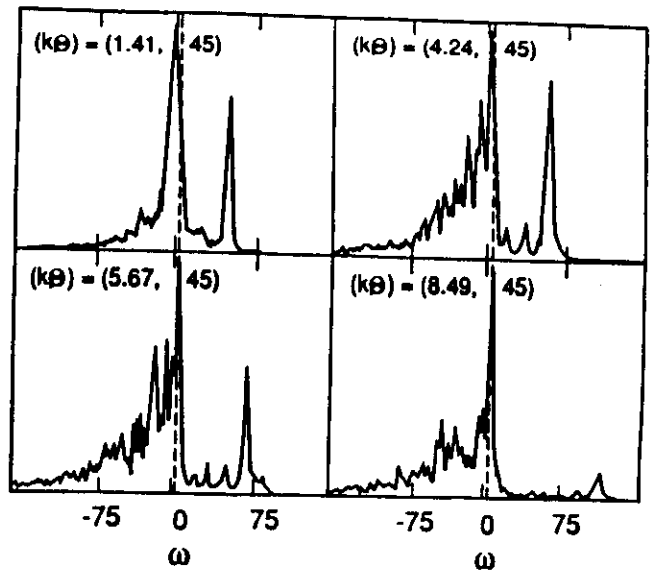

Fig. 8

Power spectra $|E(\underline{k},\omega)|^2$

$E_0=1.2$, $\omega_0=5$, $\omega_c/\omega_p=0.2$, $L_x=L_y=2\pi$, $M=1836$. Spectra are smoothed over an angular frequency interval $\Delta\omega=\pi$. Spectra intensity scales are arbitrary. The spectra are for various values of (k,θ). Because of a numerical coincidence, when these results are scaled to the more realistic value $M=9\times1836$, the frequency scale can also be read as kHz of frequency (not angular frequency).

The peaks arise from a modulation of the spectrum with an angular frequency $\Delta\omega = 2\pi/\tau_c$ where τ_c is the caviton lifetime as measured by the width in time of the total electrostatic energy pulse, $|h_0(t)|^2$, shown in Fig. (4). This is the same kind of modulation that arises in the spectrum of a single square wave pulse. Let us assume that the early-time spectrum from low-duty-cycle experiments can be identified with the incoherent average $(|\varepsilon(k,\omega)|^2)$ of single-event spectra. In this averaged spectrum the individual spectral peaks may be smeared out but it is reasonable to assume that the half-power frequency width is approximately that of the first and strongest maximum of the single-event spectra. Application of this argument to the data of Djuth, Gonzales, and Ierkic[13] in this regime – e.g., their Figure 4 – leads also to a value $\tau c \sim 1 \pm 0.05$ ms. The k dependence in this model arises from the k dependence of the eigenfunction, $e_0(k,t)$; for a localized state with $k\delta_0(t)$ we expect that $e_0(k,t) \sim \delta_0^{D2}(t)$ exp $(-k\ \delta_0(t))$. For increasing k, smaller values of $\delta_0(t)$ are favored and these correspond to more tightly collapsed states with more negative frequencies.

The free-mode peak observed in Figure 6 is, of course, not seen in this simplified scalar model calculation since it neglects all of the excited states. The free mode excitation in the scalar model is treated below. The behavior near $\omega = 0$, including the shift of the maximum peak with k, is also different in the scalar model than in the D = 2 Zakharov simulation of Figure 6. The inclusion of excited states in the scalar model brings the results into closer qualitative agreement. In the case of overdense drive $\omega_0 < 0$, this single state model agrees well with the complete Zakharov simulations.

The Fourier transform of E(r,t) is given by $E(k,\omega) \simeq \int dt \exp i\ (\omega t + \Phi_0(t))\ |h_0(t)|\ e_0(k,t)$ where Φ_0 is the phase of $h_0(t)$. For large negative ω we can make asymptotic estimates based on a stationary phase evaluation of the time integral; the stationary phase points $t = t_S$ occur approximately where $\omega = -\dot{\Phi}_0(t_S)$. From Fig. 2 we see that the ground state has large negative phase velocities where $\dot{\Phi}_0(t) \to -\lambda_0(t)$ as $t \to t_c$ and can satisfy the stationary phase condition. In this temporal regime one comes closest to the self-similar scaling for the collapsing state: $e_0(rt) = \delta_0(t)^{-D/2}\ \Psi_0(r/\delta_0(t))$ with the spatial Fourier transform $e_0(k,t) = \delta_0(t)^{D/2} \cdot \int d\xi\ (\exp - ik\delta_0\xi)\Psi_0(\xi)$. The self similar behavior is $\delta_0(t) \sim (t_c - t)^{2/D} \sim \lambda_0(t)^{-1/2}$ where t_c is the collapse time. Using these behaviors in the stationary phase evaluation of the Fourier integral we find the asymptotic behavior

$|E(k,\omega)|^2 \sim |\omega|^{-(1+3D/4)}$ as $\omega \to -\infty$. This asymptotic prediction is observed in the D = 2 vector Zakharov simulations and in the scalar simulations to an accuracy of 10%.

The single event spectra are an interesting property of the caviton cycle and should in principle be observable in laboratory experiments such as those of Cheung and Wong[27] and in local rocket-borne diagnostics of the heated ionosphere.

In the ISR experiments, however, the spectrum is the result of about 10^8 events and the question of caviton-caviton correlations becomes important. In general if the events are correlated, (4.5) is replaced by

$$(|\underline{E}(\underline{k},\omega_t|^2) = \sum_i^N |\underline{\varepsilon}_i(\underline{k},\omega)|^2$$

$$+ \sum_{i\neq j}^N \sum^N exp\ i[\underline{k}\cdot(\underline{x}_j - \underline{x}_i) - \omega(t_j - t_i)]$$

$$\cdot\ \underline{\varepsilon}_i(k,\omega)\cdot\underline{\varepsilon}_j^*(k,\omega) \qquad (4.7)$$

The second or "coherent" term in this equation has N^2 potential contributions and so could have a potent effect on the spectrum if events are correlated. We have a limited theoretical understanding of correlations at this point of our research, but recent experimental evidence from Cheung et al.[14] strongly supports the importance of correlations.

A possible model of the effect of correlations is to assume that the dispersion in the single event transform $\underline{\varepsilon}_i(\underline{k},\omega)$ is small from event to event. This is true in the scalar model calculations and has been seen in the full vector simulation; especially in the case of overdense drive. Formally, this assumption is equivalent to writing $\underline{\varepsilon}_i(\underline{k},\omega) = \underline{\varepsilon}(\underline{k},\omega) + \delta\underline{\varepsilon}_i(\underline{k},\omega)$ where $\underline{\varepsilon}$ is the average over many events and $\delta\underline{\varepsilon}_i = 0$. If we assume $|\delta\underline{\varepsilon}_i|^2 << |\underline{\varepsilon}|^2$ we can write

$$(|\underline{E}(\underline{k},\omega)|_t^2 \simeq \langle|\rho(\underline{k},\omega)|^2\rangle|\underline{\varepsilon}(\underline{k},\omega)|^2 \qquad (4.8a)$$

where

$$\rho(\underline{k},\omega) = \sum_{i}^{N(T)} exp\, i[\omega\, t_i - \underline{k}\cdot\underline{x}_i] \qquad (4.8b)$$

This quantity is just the space-time Fourier transform of the caviton event density

$$\rho(\underline{x},t) = \sum_{i}^{N(T)} \delta^D(\underline{x}-\underline{x}_i)\delta(t-t_i) \qquad (4.9)$$

Eq. (4.8a) shows that in this approximation the single event spectrum $|\underline{\mathcal{E}}(\underline{k},\omega)|^2$ is modulated by the correlation or structure factor: $\langle|\rho\,(\underline{k},\omega)|^2\rangle$.

We will argue in more detail in Sec. 6 that the increasing sharpness of the ISR spectrum observed by Djuth et al.[13] which develops a few ms after heater turn on or for low duty cycles is a result of the development of caviton correlations. The wave length of 35 cm probed by the ISR radar is about 70 λ_D and is comparable to our estimates of intercaviton spacing. Thus the spatial structure factor

$$\sum_{ij} exp\, i\,\underline{k}\cdot(\underline{x}_i - \underline{x}_j)$$

might be probed near a maximum if the cavitons have some quasi-regular arrangement. If the events are also correlated in time, the effect of correlations are more potent, as discussed in Section 6.

5. SENSITIVE DEPENDENCE ON $\omega_H - \omega_P$: OVERDENSE DRIVE AND PERSISTENCE OF CORRELATION:

As discussed previously the principal effects of a slowly varying density profile can be modeled by letting the heater amplitude E_0 be a function of space reflecting the Airy pattern of the heater and by letting $\tilde{\omega}_0 = \omega_H - \omega_P$ be a function of space to account for the mismatch between the heater frequency and the local plasma frequency. In this section we will examine the dependence of the turbulence properties on $\tilde{\omega}_0$. If we assume that the electron density profile is smooth and monotonic we can relate changes in $\tilde{\omega}_0$ to changes in altitude.

In Figure 9 we plot the total time-averaged Langmuir energy per unit volume (area) (W) (4.7), and the effective dissipation rate $R_d = \nu_{eff}|E_0|^2$ density versus ω_0 for $E_0 = 1.2$, $\omega_c/\omega_p = 0.1$, $\nu_i = 0.9$. We see a dramatic increase in R_d as ω_0 becomes negative. Negative values of ω_0 are only of interest in the evanescent region of the pump wave, $z > z_c$, or if there are domains of over-dense plasma whose spatial dimensions are smaller than the skin depth of the heater wave, $\ell \sim c/\omega_p\,(1 - \omega_p^2/\tilde{\omega}^2)^{-1/2}$ so that the heater can penetrate.

This increase of R_d is a sign of greatly increased caviton activity. This is easily understood from the nucleation picture: For $\omega_0 < 0$ the relaxing density well remaining from a previous burnout comes earlier into resonance with the pump and therefore at a relatively deeper depletion compared to the $\omega_0 = 0$ case. Thus at the time of closest resonance $\lambda_\nu \sim \omega_0$ the eigenfunction $\underline{\varepsilon}_\nu(\underline{x},t)$ is more confined. The caviton cycle presumably will be more stable and less effected by neighboring cavitons in this more confined caviton cycle. Thus we expect more rapid caviton cycles, i.e., smaller τ_c, with less energy carried into collapse. The fact that (W) increases by 50% and R_d increases by about 300% as ω_0 goes from +5 to −5 is consistent with this picture. The overdense drive $\tilde{\omega}_0 < 0$ is much more efficient in the nucleation of cavitons.

An important observation of the scalar, local caviton model discussed in Section 3, is that the single event functions $\hat{\varepsilon}_i(\underline{x} - \underline{x}_i, t - t_i)$ are phase locked to the pump. Thus it was more convenient to replace these functions in (3.1) by $\exp - i\omega_0 t$ $\varepsilon_i(x - x_i,\ t - t_i)$; that is to explicitly separate out the pump phase. [See also (3.11).] Another way to look at the problem is to rewrite (2.9) in terms of $\hat{E}(\underline{x},t) = \exp(-i\omega_0 t)\, E(\underline{x},t)$, i.e., to envelope around the pump frequency. As an equation for $\hat{E}$ the equations are autonomous, i.e., the drive term has no explicit time dependence but an additional term, $\omega_0\,\hat{\underline{E}}(\underline{k},t)$, appears on the left hand side of (2.10a). The result of this is that the single caviton spectra for $\omega_0 \neq 0$, $|\underline{\mathcal{E}}(\underline{k},\omega)|^2$, have their spectral energy mainly for $\omega < \omega_0$. The eigenvalue trajectories versus time have the property that they reverse near the resonance $\lambda(t) \leq \omega_0$ where the PMF reverses the relaxation of the density well.

This picture is confirmed in detail in the isolated scalar model calculations. In Figure 10 we show the behavior of the dissipation rate $R_d \equiv \nu_{eff}|E_0|^2$ and the

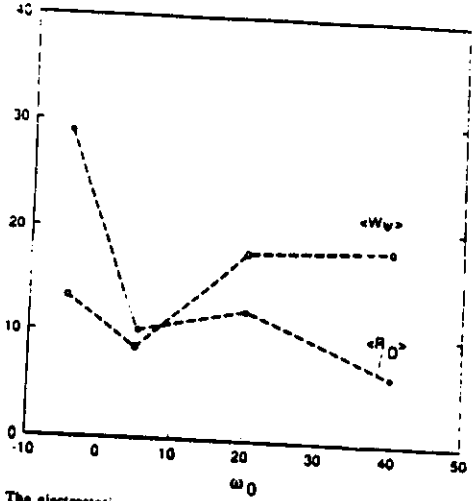

Fig. 9

The electrostatic energy density (W_ψ) and the dissipation per unit area per unit time, $P_d = 2\Gamma_k \omega_r(k)|E(k)|^2 = \nu_{eff}|E_0|^2$, versus the relative heater frequency. $E_0 = 1.2$, $\omega_r = 0.9$, $m_e/m_i = 1836$.

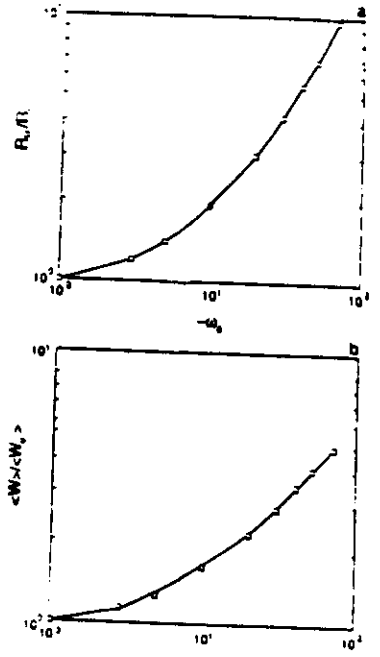

Fig. 10

D=3 scalar model results for dissipation rate per unit volume R_d and Langmuir energy per unit volume W versus ω_0 for underdense driving, $\omega_0 < 0$. Parameters: $E_0 = 5.0$, $m_e/m_i = 2 \times 10^{-4}$, $\omega_r = 0.9$

total Langmuir energy/unit volume (W) versus ω_0 in this model. Again we see a dramatic increase in caviton activity as measured by R_d as ω_0 becomes increasingly negative. Since this model contains only the ground state it becomes unreliable for $\omega_0 > 0$. In these calculations we also find that the energy per caviton taken into collapse, N_{max}, decreases as ω_0 decreases; however, the density of cavitons $\rho \sim \delta^{-3}$ increases in such a way that $\langle W \rangle \sim \delta^{-3} N_{max}$ increases as ω_0 decreases.

These observation have led us to examine more closely the properties of the turbulence for $\omega_0 < 0$. A very important new property emerges which is not evident in Figure 9. In the regime $\omega_0 < 0$ there are significant hysteresis effects; this means that the turbulent state depends very much on initial conditions or at least that the memory of initial conditions decays in time much more slowly than in cases where $\omega_0 < 0$. For example, if $-\omega_0 > |E_0|^2$ the system is modulationally stable and cannot be excited to a nonlinear or turbulent state from quiet (e.g., thermal) initial conditions. On the other hand, the turbulence is sustained by nucleation from turbulent initial conditions for the data points at $\omega_0 = -5$ in Figure 9 where $E_0 = 1.2$. This behavior is not unexpected in light of the arguments made above for caviton cycles which are more stable and less effected by neighboring cavitons when $\omega_0 < 0$. To obtain the data points in Figure 9 we chose initial conditions in which the initial caviton locations and cycle phases did not have any particular order. (In fact, the initial state was the final state of another simulation with $\omega_0 = 0$ which also had disordered turbulent initial conditions.)

This hysteresis greatly increases the parameter space which needs to be studied since now we need to specify the detailed initial conditions. We are far from a complete understanding of the basins of attraction of various initial conditions. However, we wish to present here one case which has interesting properties and has led us to consider the perfectly correlated, alternating lattice models postulated in the following section. This example is one of a class of simulations in which cavitons initially arranged in a regular array of sites persist at these sites, their cycles become very stable and become phase locked to one another in various temporal patterns.

In Figure 11 we show the initial locations of two density cavities which resulted from previous collapses and in which the initial electric field fluctuation is set to zero. This is the initial state for a simulation with $E_0 = 1.2$ and $\omega_0 = -25$ in scaled

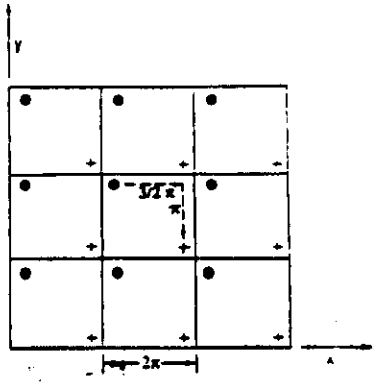

Fig. 11

Two dimension simulation of alternating lattice model. Caviton locations marked ● are τ/2 out of phase with locations marked +. The caviton cycle period is τ. The central square is the simulation cell. The other cells are implied by the periodic boundary conditions. The o's and +'s denote the initial caviton locations which do not change for $\omega_0 = -25$ or $\omega_0 = -15$. Other parameters: $E_0 = 1.2$, $v_i = 0.9$, $m_i/\eta m_e = 1846$.

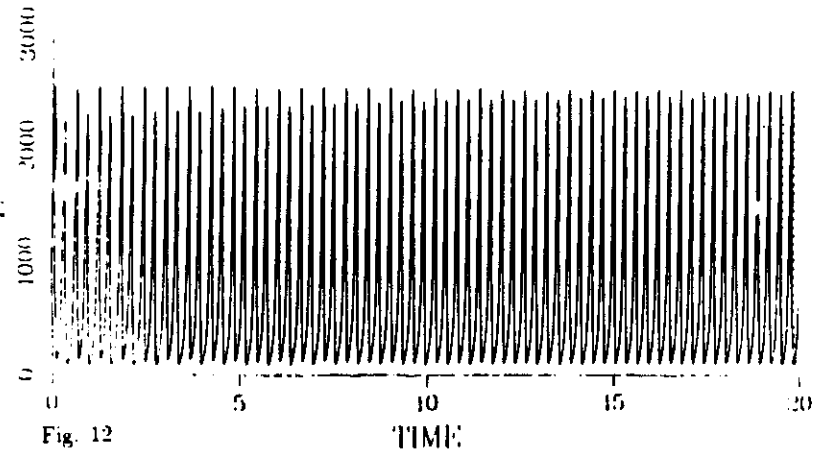

Fig. 12

The maximum $|E(x,t)|^2$ over the simulation box versus time for the coherent alternating lattice simulation described in Fig. 11 The single caviton power spectra in Figures 13 and 14 are calculated over the time interval indicated by the dashed lines.

units. This value of ω_0 corresponds to a domain in physical units which is about 1% overdense. In Figure 12 we show the time series of the maximum value of $|E(x,t)|^2$ versus time as the system evolves into a periodic pattern. As time increase each evolves into a strict limit cycle with period $\tau = 0.59$ with the cycles at the two sites becoming $\tau/2$ out of phase with one another. We will generalize this behavior in the alternating lattice models postulated in the next section.

In Figure 11 we also show the extended spatial periodicity implied by our periodic boundary conditions. This shows that the simulation is equivalent to two interpenetrating square lattices in which the ● positions are all in phase but are $\tau/2$ out of phase with the + positions which themselves are all in phase. Examples of the computed spectra are shown in Figure 13 for $\theta = 0$ and $\theta = 45°$.

In Figure 13 the single event spectra are also shown for the same values of (k,θ). These are easy to isolate from a single cycle at a given site. According to (4.8a) the single event spectrum modulates the spectrum of the structure factor. Comparison of the complete spectra and the single caviton spectra in Figure 13 verifies this.

In Figure 14 we show the ion line spectra obtained from the same simulations. Note, in the cases in which the plasma line spectra in Figure 9 has peaks at odd multiples of $2\pi/\tau$ (i.e. cases a and d) structure, the ion line consists of a symmetrical peak around $\omega = 0$ (corresponding to $\tilde{\omega} = \omega_H$) and two displaced peaks at $\omega = \pm 2\pi/\tau$. These two displayed peaks are shifted by exactly the same frequency as the "decay line" peak in the plasma line spectra in Figure 13 a and d. This correlation of frequency shifts in the plasma line and ion line spectra has often been offered as evidence of the parametric decay instability; here we see that the same spectral correlation can arise from completely different physics!

The very sharp spectra in these examples arise from nearly perfect correlations which persist over many caviton cycles - about 50 cycles in the simulations. Note in Figures 9.5a and d, which have prominent peaks in the 1:3:5 pattern, that there are also weak peaks at $\omega = 0$ and $\omega = m(2\pi/\tau)$ where m is odd. These arise from slight deviations from the perfectly correlated model. The weak peak at $\omega = 0$ would contribute to the "OTSI" line. We will argue in the next section that these spectral components could also arise from higher order (e.g., $|\nu| = 2$ Bragg resonances from domains with larger lattice spacings, a, corresponding to regions with weaker E_0 which produce weaker plasma line signals.) We also argue there

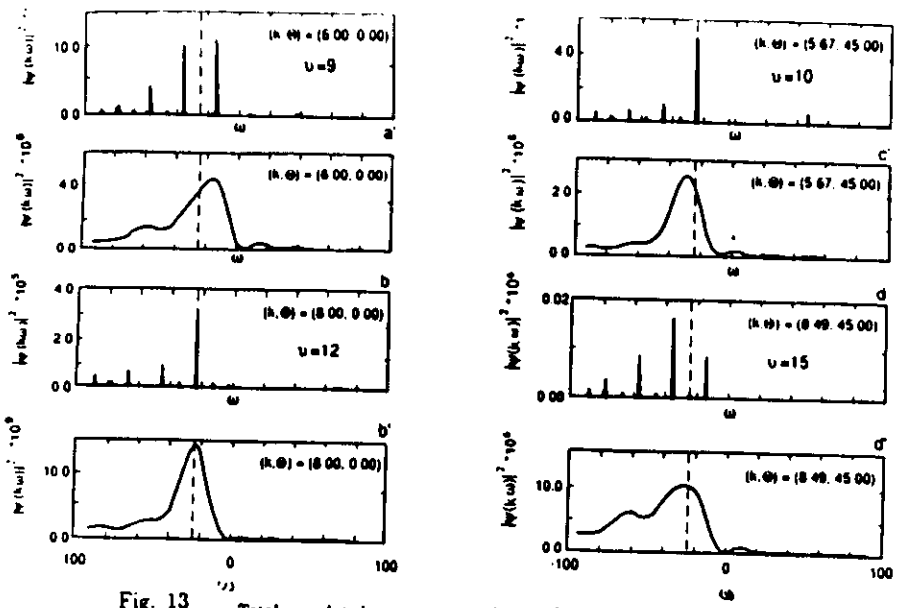

Fig. 13 Total correlated power spectra $|E(k,\omega)|^2$ and single caviton spectra $|c(k,\omega)|^2$ for the coherent alternating lattice for various values of (k,θ). Showing spectra for even and odd values of $\nu = (1/2\pi)\, k \cdot d$.

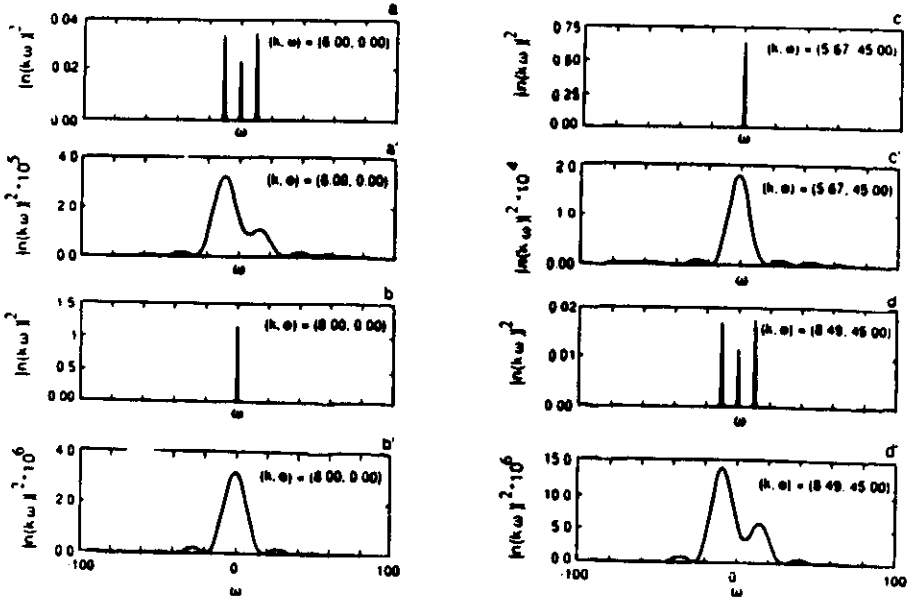

Fig. 14 Ion line spectra $|n(k,\omega)|^2$ for the coherent alternating lattice simulation. Both the total spectrum and the single caviton spectrum are shown.

that the "OTSI line" would also have important contributions from domains which are temporally correlated but not spatially resonant. These models again suggest how caviton correlations might produce spectra which mimic the "decay-line" (and its anti-Stokes partner), the cascade and the "OTSI line."

These preliminary results encourage us to believe that the SLT model with correlations might explain all the observed features of the ISR spectra. We believe there is overwhelming theoretical and experimental evidence that the conventional parametric instability theory cannot do the same.

Much remains to be done to understand theoretically how (or even if) such correlations develop from physically realistic initial conditions in SLT. Until this is done or until experiments directly measure such caviton correlations these correlation models must be regarded as postulates which appear to be consistent with ISR observations and with our limited theoretical understanding. The theoretical understanding, based mainly on simulation results for the case of overdense driving, can be summarized as follows:

i.) Temporal correlations at a given site devleop, on the time of a cycle period, into stable limit cycles.

ii.) Temporal correlations between sites evolve more quickly than spatial correlations between sites.

iii.) Some spatial patterns appear to be stable equilibrium arrangements with definite temporal correlations between sites.

iv.) Those patterns which are not stable equilibria evolve to stable patterns on an experimentally relevant time scale - say tens of ms.

We have discussed (i) at some length above. An example of (ii) is the simulation discussed in relation to Figure 11 in which cavitons at neighboring sites became anti-correlated in time. Points (iii) and (iv) (as well as other examples of (i) and (ii) are based on simulations which we will not present here. This work is part of our continuing research.

Other questions remaining to be addressed concern how the overdense regions are formed and how the turbulence is excited in these regions. We note that the existence of a modulational instability (or PDI) is inconsistent with overdense drive if $-\omega_0 > |E_0|^2$. Therefore, in a preexisting overdense region the only way the heater

can excite the turbulence is through direct nucleation in preexisting density cavities as discussed in Section 3. [The direct nucleation by the pump might be enhanced by free modes driven up by direct conversion of the heater on preexisting density fluctuations. These free modes can also provide a nucleation source for localized states as discussed in Section 7.]

Another scenario is that the turbulence is initially excited in underdense regions which subsequently become overdense in intermediate scale (10-100 m) density modulations resulting perhaps from thermal instabilities that develop on an intermediate time scale (say tens of ms). The adiabatic increase of the density to an overdense condition would then "freeze in" local caviton cycles which might then evolve into a spatially correlated state. Density increases of 1% or less can lead to overdense regions in parameter ranges comparable to the simulations discussed above.

The space and time scales (10-100 m, tens of ms) of the density modulations or irregularities invoked above are smaller than usually calculated for thermal self-focusing or related instabilities which usually consider ordinary Ohmic heating.[28,29,30] However, in the turbulent region the effective dissipation rate (into hot electrons), ν_{eff}, is much larger than the ordinary collision frequency. The space and time scales of the thermal instabilities depend on collision frequency as ν_{ei}^{-2} e.g. (see Rubenchik and Turitsyn[31]) which would imply that they scale roughly as ν_{eff}^{-2} in the case of turbulent dissipation. Thus the space-time scales of the thermal instabilities in the regime of turbulent dissipation could be several orders of magnitude smaller than in the case of Ohmic dissipation. A more detailed analysis of these effects will be given elsewhere.

Our current research is focused on gaining a better perspective on the parameter regimes of E_0, ω_0 and ν_i for which correlations persist. We have verified, for example, that the behavior seen in Figures 13 and 14 is qualitatively the same when ω_0 is changed to $\omega_0 = -20$. In this case the single caviton period increases to $\tau = 0.62$, which is qualitatively what we expect from the nucleation model. For $\omega_0 = -15$, on the other hand, the two cavitons become synchronous with period $\tau = 0.69$.

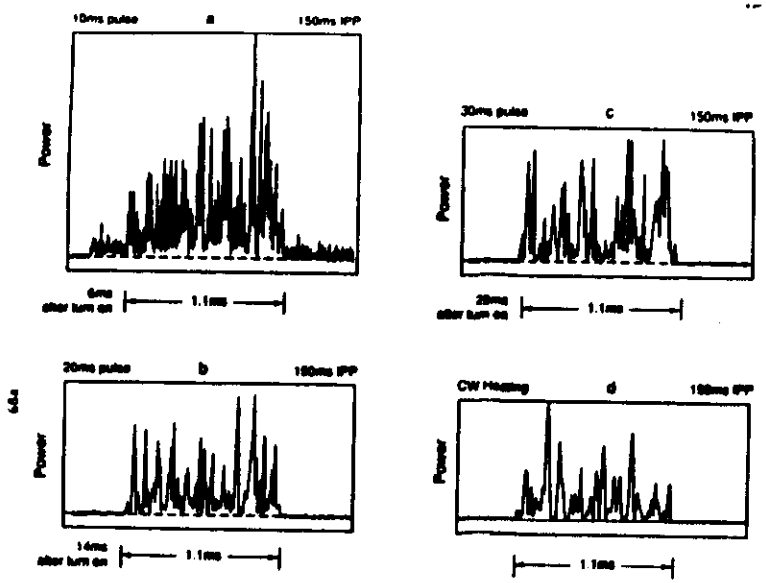

Fig. 15 **Plasma line power vs time in single radar pulses of length 1.1 ms a-b at varying times after turn-on of heater pulse. (a) 6 ms after turn on of 10 ms heater pulse, (b) 14 ms after turn on of 20 ms heater pulse, (c) 29 ms after turn on of 30 ms heater pulse; 150 IPP in each case, (d) CW heating. From Cheung, Sentoru, Tanikawa, and Wong (1988).**

6. CAVITON CORRELATIONS

Compelling evidence that cavitons are strongly correlated with one another is contained in the data obtained by Cheung et al.[14] in low duty cycle experiments, described above, at Arecibo. Plasma line data was obtained from single radar pulses of about 1 ms duration. Figure 15 shows the typical time evolution of the total plasma line power over a radar pulse duration with a time resolution of about 1 μs. It shows a strongly modulated signal with peaks about 0.025 ms wide separated by about 0.05 ms. The widths of these peaks are comparable to that of the peaks in total electrostatic energy, $|h_0(t)|^2$, versus time in Figure 2, as estimated from the scalar simulations in Section 3 for ionospheric heating conditions. Similar looking single-radar-pulse time series are observed in 1 ms time intervals both early and late in the heater pulse in the low duty cycle experiment and in CW heating experiments. These appear to show that the period of the modulations and the depth of the modulations increase with the time elapsed after the onset of heating; see Figures 15. Time series averaged over many (~100) radar pulses are relatively smooth showing little of the modulation of single pulses.

This signal is not consistent with a system of uncorrelated cavitons. Suppose the caviton "firing" times t_i (see (5.7)) are uniformly distributed over the radar pulse interval T and that the mean temporal spacing between events, T/N, is much less than the caviton period τc. Then at each instant of time the signal can be approximately representd as $\underline{E}(kt) \cong \sum_i |a_i(t)| \exp i(\phi_i(t))$ where the sum is over the many overlapping events at time t which have slowly varying amplitudes $|a_i(t)| = \underline{e}_o(k,t\text{-}t_i)|h_i(t\text{-}t_i)|$ and rapidly varying phases $\phi_i(t) = \Psi_i + \Phi\ (t\text{-}t_i)$. The phase is composed of the spatial part $\Psi_i = \underline{k}.\underline{x}_i$ which for this argument we take to be uniformly distrubuted in $[0,2\pi]$ and the phase of the caviton $\Phi(t\text{-}t_i)$ which we studied in Section 5. Considering the rapid variation of Φ with time found in these studies it is reasonable to consider that the total phase ϕ_i is also uniformly distributed in $[0,2\pi]$. At each instant of t the complex vectors in the sum on i represent a random walk in the complex plane over a large number of steps N. The resulting probability distribution of $P(|E|^2)d|E|^2$ that $|E|^2 = |E^2(k)|^2$ lies between $|E|^2$ and $|E|^2 + d|E|^2$ found from a well-known application of the central limit theorem to be $P(|E|^2) = (|E|^2)^{-1} \exp(-|E|^2(|E|^2))$ where $(|E|^2) \sim N(|a|^2) = N(|h|^2 e_o^2(k))$. Thus there is a significant probability of configurations with small resultant

values of $|E|^2$ (say $|E|^2 < (|E|^2)$). Next we ask how quickly these configurations change. If the phases ϕ_i are uniformly distributed and the phase velocities, $\dot{\phi}_i = \dot{\Phi}\ (t\text{-}t_i)$, which are independent of the spatial phase Ψ_i and are therefore taken to be uniformly distributed independently from the ϕ_i's, we can compute the following averages:

$$(|E|^2) = N|a|^2, (\frac{d}{dt}|E|^2) = 0 \quad and \tag{6.1}$$

$$\frac{([\frac{d}{dt}|E|^2|^2)}{(|E|^2)^2} = 2[(\dot{\Phi}^2) - (\dot{\Phi})^2] \tag{6.2}$$

in terms of the mean and mean square phase velocities. From studies, such as those in Section 3, of the temporal histories of the phase velocity $\dot{\Phi}$ during the caviton cycle we see that $[(\dot{\Phi}^2) - (\dot{\Phi})^2] \sim (\dot{\Phi}^2) >> \tau_c^{-2}$. Thus the time variation of $|\underline{E}(k)|^2$ for a system of uncorrelated cavitons should exhibit strong modulations which change on a time scale very short compared to a caviton lifetime. The observed power time signals, in Figure 15 on the other hand, except perhaps for the earliest time delay of 6 ms, shows a much longer modulation time period which is close to the predicted caviton lifetime $\tau_c \sim 0.05$ ms.

This signal is consistent with the local caviton model where there are significant correlations between events. If out of a total of N there are N_c correlated events the ISR signal from the correlated events is proportional to $N_c{}^2$ while that from the uncorrelated events is proportional to $N\text{-}N_c$. If the ratio of the modulation peaks in the power signal in Figure 15 to the background are estimated to be 100 to 1 then we have roughly $N_c{}^2/(N\text{-}N_c) \sim 10^2$ so with $N \sim 10^8$ we find $N_c \sim 10^5$. Thus if only 0.1% of the total events are correlated a dramatic effect on the spectrum can be expected! This argument seems quite general and independent of the details of the correlations. The observed real-time backscattered power signal in a single radar pulse, from the perspective of the local caviton model, leads then to the conclusion that many collapse events are coincident in time. This conclusion rests on our estimates for N and for the caviton lifetime τ_c. From this point of view each peak in the time series is a resultant macrofluctuation of many coincident collapse events.

Further evidence of correlations is obtained in these experiments from the power spectra of single radar pulses. The single pulse observed spectra show a much finer

frequency structure. We can associate this fine "line" structure with a discrete set of temporal events; each "event" now includes the correlated collapse of many cavitons with an average event spacing in time of about 0.04-0.05 ms. Our simple estimate above implies that each event involves the order of 10 $\sqrt{N}$ correlated cavitons. A detailed analysis of the single radar pulse spectrum is given in ref. 1.

We can summarize the comparison between the local caviton model, the D = 2 simulations and the short time scale ISR experiments as follows:[1]

1.) The many pulse averaged observed spectra agree in detail with the smoothed simulation spectra. The main energy containing portion of these spectra occur for $\omega < 0$ and there is a free mode peak for $\omega > 0$.

Examples of experimental spectra from Cheung et al.[14] are shown in Figure 16. Examples of smoothed simulation spectra including geomagnetic field effects are shown in Figure 7 taken from DuBois et al.[1]

2.) The local caviton model accounts for the $\omega < 0$ spectral features as arising from the nucleation-collapse-burnout caviton cycle as discussed in Section 4.

3.) Associated with each caviton cycle a nearly free Langmuir wave packet is radiated away from each caviton site. This is discussed in detail in Section 10. The free mode peak occurs at a frequency $\tilde{\omega}_f = \omega_p[1 + (3/2)(\tilde{k}\lambda_p)^2 + (1/2)(\tilde{\omega}_c/\omega_p)^2 \sin^2\theta]$ associated with a free Langmuir wave for which $\tilde{\omega}_f > \tilde{\omega}_H$ yet is a distinct signature of the collapse process.

4.) The single pulse spectra and power time series are consistent with strong temporal coherence or synchronism in which blocks of many cavitons fire nearly simultaneously. The resulting line structured spectra is consistent with the model of a structure factor derived from a discrete set of macroevents that occur during a 1 ms radar pulse.

In several sets of observations[31,12,13,14] sharp spectral peaks are observed to develop as the time delay of the radar pulse is increased following the onset of the heater pulse. In Figure 17, a 50-pulse average spectrum is shown in which the radar pulses occur 29 ms following the onset of a 30 ms heating pulse with a 150 ms IPP. This spectrum shows features observed in many previous long-time experiments[32] consisting of a main "decay line" peak lying about 3.0 ± 0.5 kHz below the heater frequency and two "cascade" peaks lying further below the heater frequency by 10.0

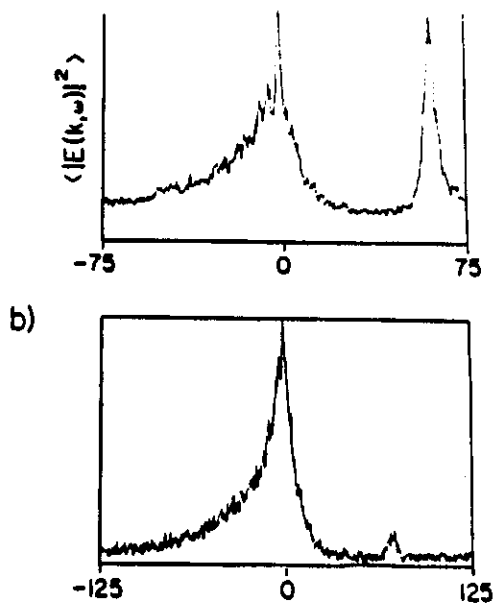

Fig. 16

Experimental spectra. (a) Heater pulse width 10 ms. IPP 150ms, f_H = 7.3 MHz spectra taken in 1.1 ms inte.· als delayed 4 ms from onset of heating pulse. Note the free mode peak at ~ 72 kHZ above the heater frequency which is 256 on the scale. (b) Heater pulse width 10 ms, IPP 150 ms, f_H = 7.3 MHz spectral delayed by 1.5 ms from onset of heating. Free mode peak at 52 kHz. From Cheung et al. (1989).

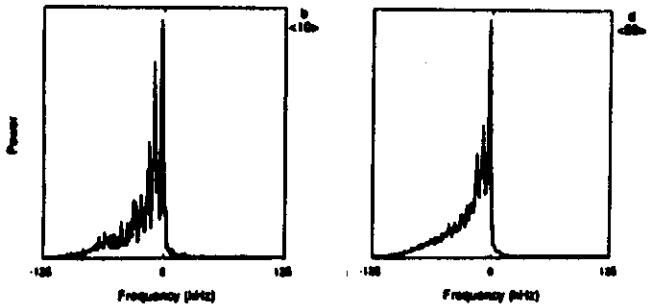

Fig. 17

Plasma line spectra for 30 ms. heater pulses with 150 IPP at 7.3 Mhz and radar pulse delayed by 29 ms after onset of heater pulse. averages over 35 and 50 radar pulses, respectively.

± 0.5 kHz and 16.0 ± 0.5 kHz, respectively. This approximate "1:3:5" pattern of frequency displacements is sometimes associated with a weak turbulence cascade.[32]

The question to concern us next is whether such a spectral pattern can be explained in terms of caviton correlations? We will first postulate a class of strongly-correlated models which are motivated by the simulation results discussed in the previous section for the case of overdense drive. We found that for overdense driving where $\tilde{\omega}_H > \omega_p$ very stable cycles can be found with cavitons in ordered spatial arrays. We also will assume for reasons discussed in Section 3 that the spacing between cavitons decreases like E_0^{-1} where E_0 is the local strength of the heater electric field.

We will assume that the cavitons tend to order themselves in a regular three-dimensional lattice. In the ionosphere application, because the heater field varies within the radar observed region, due to the antenna pattern and the altitude dependent Airy pattern, the spacing, a, of cavitons in the lattice varies on a scale large compared to a. In regions of most intense E_0, a will be smallest. The orientation of the lattice may also vary within the observed region. Our scalar model simulations show that for $E_0 \simeq 0.5$ V/m the maximum isolated caviton size is about 40 λ_D so we might expect an intercaviton spacing a > 80-100 λ_D or about 40-50 cm. At Arecibo the radar wavenumber is about 2π (35 cm)$^{-1}$ which means that low order Bragg scattering from such a lattice is possible with small adjustments of the lattice spacing which could arise through variations in E_0. We imagine that the observed region of the heated ionosphere contains domains of ordered cavitons whose lattice spacing and orientation varies from domain to domain. These spatially and temporally ordered domains take some time to organize themselves after the onset of heating. We have some preliminary simulation evidence for this which we presented in Section 5.

In each domain the cavitons are located at sites in a spatially periodic lattice. Each caviton undergoes a periodic cycle of nucleation-collapse-burnout, etc. with period τ but nearest neighbor cavitons have their cycles displaced by $\tau/2$ from each other. (We have presented evidence that in certain regimes nearest neighbors tend to be out of phase in Section 5.)

We can consider a domain to consist of two interpenetrating synchronous lattices whose cycle time differs by $\tau/2$. Thus we can write

$$\rho(\underline{k},\omega) = \sum_{m=1}^{M} e^{im\tau\omega} Z(\underline{k}) + \sum_{m=1}^{M} e^{i(m\tau+\frac{1}{2}\tau)\omega} e^{-i\underline{k}\cdot\underline{d}} Z(\underline{k}) \qquad (6.3a)$$

where again

$$Z(\underline{k}) = \sum_{n}^{N_d} e^{-i\underline{k}\cdot\underline{x}_n} \qquad (6.3b)$$

but now we consider the locations $\underline{x}_n$ to lie on a perfect lattice. The points $\underline{x}_{n\prime}$ in the second lattice are related to the points $\underline{x}_n$ in the first lattice by a displacement, $\underline{x}_{n\prime} = \underline{x}_n + \underline{d}$.

We can generally represent a lattice site $\underline{x}_n$ in terms of three elementary lattice basis vectors $\underline{a}_1$, $\underline{a}_2$, $\underline{a}_3$ which uniquely specify the lattice.

$$\underline{x}_n = n_1\underline{a}_1 + n_2\underline{a}_2 + n_3\underline{a}_3 \qquad (6.4)$$

where n_1, n_2, n_3 are integers. For simplicity we chose the displacement of the second lattice to have the symmetric form:

$$\underline{d} = \frac{1}{2}(\underline{a}_1 + \underline{a}_2 + \underline{a}_3) \qquad (6.5)$$

We assume the two lattices are the same except for the displacement $\underline{d}$ which must have a special relation to the symmetry of these lattices. It is easy to carry of the sum on m and to find

$$|\rho(\underline{k},\omega)|^2 = 4\cos^2\frac{1}{4}(\omega\tau - 2\underline{k}\cdot\underline{d})\frac{\sin^2\frac{1}{4}M\omega\tau}{\sin^2\frac{1}{2}\omega\tau}|Z(\underline{k})|^2 \qquad (6.6)$$

This structure factor has temporal resonances at

$$\omega = 2\pi m \quad (m = 0 \text{ or any integer}) \qquad (6.7)$$

and spatial (Bragg) resonances at a set of wave vectors

$$\underline{k} = \underline{K}_\nu \qquad (6.8)$$

for which exp i$\underline{K}_\nu \bullet \underline{x}_n = 1$ for all $\underline{x}_n$ in the lattice. These resonant wave vectors $\underline{K}_\nu$ are known as "reciprocal lattices" vectors in solid state physics. (All of the lattice concepts which we use here are treated in texts on elementary solid state physics, e.g., Kittel.[33] When <u>both</u> of these resonance conditions are satisfied it is easy to see that $|\rho(\underline{k},\omega)|^2$ reaches it maximum correlated value proportional to $(M\ N_d)^2$ where $M\ N_d = N_c$ is the total number of events in the observed space-time volume. In the specific models we will discuss below we find

$$2\underline{K}_\nu \bullet \underline{d} = 2\pi\nu \tag{6.9}$$

where ν is an integer. Therefore when <u>both</u> the spatial and temporal resonance conditions are satisfied the modulating factor $\cos^2 1/4(\omega\tau - 2\underline{k}\bullet\underline{d})$ has its maxima at $(\omega\tau)_{max} - 2\ \underline{K}_\nu \bullet d = 4\pi\ell$ (ℓ any integer or zero) or using (6.7) we have

$$(\omega\tau)_{max} = 2\pi(2\ell + \nu) \tag{6.10}$$

Likewise the zeroes of the $\cos^2$ function fall at

$$(\omega\tau)_{zeroes} = 2\pi(2\ell + \nu + 1) \tag{6.11}$$

Thus we have two cases:

1.) ν = odd integer where $|\rho(\underline{k},\omega)|^2$ has peaks at $\omega = (2\pi/\tau)$m where m is any odd integer

2.) ν = even integer where $|\rho(\underline{k},\omega)|^2$ has peaks at $\omega = (2\pi/\tau)$m where m is any even integer or zero.

In case 1.) $|\rho(\underline{k},\omega|^2$ has spectral peaks at ω equals (--- -5, -3, -1, 1, 3 ---) x $(2\pi/\tau)$. When multiplied by the single event spectrum, $(|\underline{\varepsilon}(\underline{k},\omega)|^2$, which has most of its energy for $\omega < 0$ the total spectrum will consist of a major line at $\omega = -2\pi/\tau$ and succeedingly weaker lines at $\omega = -3(2\pi/\tau)$, $-5(2\pi/\tau)$ etc. which is similar to the 1:3:5 structure in the observed spectra mentioned above. In addition, depending on the strength of the single event spectrum for $\omega > 0$, there may be a weak line at $\omega = 2\pi/\tau$ which would correspond to the often observed "anti-Stokes" line.[32]

Of course, when ν is zero or an even integer the spectral pattern is different with peaks at ω equal to (-6, -4, -2, 0, 2, 4, 6 ---) $2\pi/\tau$. The two classes of spectra are illustrated in Figure 18.

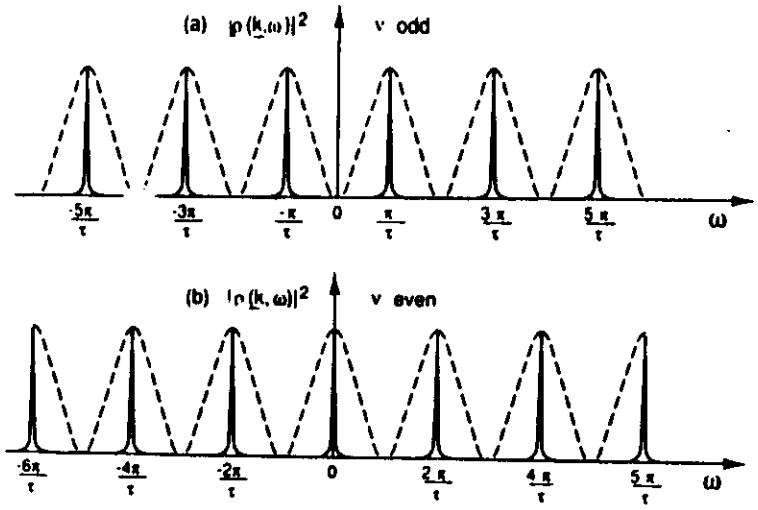

Fig. 18 Correlation spectra $|\rho(\underline{k},\omega)|^2$ for even and odd values of ν. Dashed curves are the modulating factor $\cos^2 1/2\,(\omega/2 - \underline{k}\bullet\underline{d})$ of Eq. 8.9.

For the spatial Bragg resonance the radar $\underline{k}$ must equal one of the reciprocal lattice vectors. The length of $k = \pi/\lambda_{radar}$ is fixed and we can always write the length of a reciprocal lattice vector in the form

$$|\underline{K}_\nu| = \frac{2\pi}{a} A_\nu \tag{6.12}$$

where say a is the smallest lattice dimension. The Bragg resonance condition then provides a condition on a:

$$a = \frac{2\pi}{|k|} A_\nu = 2\lambda_{radar} A_\nu \tag{6.13}$$

The direction of $\underline{K}_\nu$ which must also be in the direction of the radar $\underline{k}$. We will allow the orientation of the lattice to vary somewhat in our further discussion.

The smallest lattice spacing, which corresponds to the smallest value of A_ν consistent with the angular constraints, should correspond to the domains with the largest E_0. It is shown in ref1that the averaged plasma line power, $(P(k)) = (|\underline{E}(k)|^2)$, increases rapidly with E_0 in parameter regimes of interest. Therefore, we expect the strongest correlated signal to come from domains with the smallest resonant values of a.

A reciprocal lattice vector (RLV) can also be represented in terms of three elementary lattice vectors $\underline{\kappa}_1, \underline{\kappa}_2$, and $\underline{\kappa}_3$.

$$\underline{K}_\nu = \nu_1 \underline{\kappa}_1 + \nu_2 \underline{\kappa}_3 + \nu_3 \underline{\kappa}_3 \tag{6.13}$$

where $\underline{\kappa}_1 = 2\pi\,(\underline{a}_2 \times \underline{a}_3)\,(\underline{a}_1 \bullet (\underline{a}_2 \times \underline{a}_3))^{-1}$, $\underline{\kappa}_2 = 2\pi\,(\underline{a}_3 \times \underline{a}_1)\,(\underline{a}_1 \bullet (\underline{a}_2 \times \underline{a}_3))^{-1}$ and $\underline{\kappa}_3 = 2\pi\,(\underline{a}_1 \times \underline{a}_2)\,(\underline{a}_1 \bullet (\underline{a}_2\ \underline{a}_3))^{-1}$. From these results it is easy to show $\underline{\kappa}_i \bullet \underline{a}_j = 2\pi\,\delta_{ij}$ from which it follows using (6.10) that

$$2\underline{K}_\nu \bullet \underline{d} = 2\pi\nu \tag{6.14}$$

where

$$\nu = \nu_1 + \nu_2 + \nu_3 \tag{6.15}$$

The three shortest RLV's, corresponding to the lowest values of $|A_\nu|$, are the three basis vectors $\underline{\kappa}_1, \underline{\kappa}_2, \underline{\kappa}_3$ which correspond to the values of the triad (ν_1, ν_2, ν_2) of (1,0,0), (0,1,0) and (0,0,1), respectively. Thus for the three shortest RLV's $\nu = 1$ and so for $\underline{k} = \underline{\kappa}_1, \underline{\kappa}_2$ or $\underline{\kappa}_3$ a 1:3:5 type of spectrum is found.

The domains whose lattice spacing is small enough to achieve the strongest resonance must also have their "crystal" orientations such that the direction of k measured by the radar is nearly along the direction of one of the basis vectors $\underline{\kappa}_1, \underline{\kappa}_2$ or $\underline{\kappa}_3$. There are at least two ways to achieve this: The crystal orientations as well as the spacing may vary throughout the heated region allowing the resonance conditions to be satisfied in some local region. Another possibility is that the orientation of the caviton lattice does not vary much and the particular directions, $\theta \sim 45°$ for the Arecibo radar and $\theta \sim 0°$ for the Tromsø radar, both correspond to directions of reciprocal lattice basis vectors. A more complete discussion is given in reference 1.

Domains of coherent cavitons whose lattice spacing is not Bragg resonant for the given radar $\underline{k}$ would be expected to coexist with the Bragg resonant domain(s). Such domains will have weaker resonances at $\omega = 2\pi m\ \tau_d^{-1}$ for all m where the life time of the caviton cycle τ_d varies from domain to domain. The resonance at ω=0 is common to all domains and is not smeared out by domain to domain variations of τ_d as are the resonances for $m \neq 0$. The $\omega = 0$ resonance can be identified with what is conventionally called the "OTSI line" in ionospheric heating parlance. This line can be extremely narrow if the caviton cycles are long lived; we find $\Delta\omega \alpha \pi (M\tau_d)^{-1}$ where M is the number of cycles in the observation interval. The caviton picture provides the only nonlinear description which we know of which is capable of understanding the very narrow width of the "OTSI line" observed in the experiments of Sulzer and Fejer.[34,35]

7. RADIATION of "FREE" LANGMUIR WAVES BY COLLAPSING CAVITONS

Our studies have shown that the collapse process invariably excites "free" Langmuir waves. These manifest themselves in the "free mode" peak which occurs in all the power spectra, $|E(\underline{k},\omega)|^2$, which we have computed. As discussed in Sec. 6 there is strong evidence that the free mode peak has been observed in the short time scale experiments of Cheung et al.[14]

These free mode states are extended states whose energy is not localized at a particular point in space. A single collapsing caviton will radiate a wave packet of free modes which spread out and whose amplitudes decay geometrically (as r^{-1}) away from the excitation center of the caviton. [We use the term extended in a physical sense; to be mathematically precise boundary conditions at "infinity" must be specified. Because we are studying transient dissipative phenomena, these Langmuir fluctuations cannot explore "infinity."]

Outside of the spatial region of an isolated collapsing caviton these radiated Langmuir waves are asymptotically free Langmuir waves obeying the dispersion relation of (2.5). In a many-caviton environment, the large density fluctuations generated by collapse distort their propagation. The free mode frequencies appear to approach the dispersion relation (2.5) as k increases. For lower k values the frequencies are shifted to somewhat higher values due to the perturbation of the density fluctuations.

The generation of free modes can be understood in terms of the coupled mode amplitude equations (4.7). For simplicity we ignore the dissipative coupling (4.9b) which is not important for the k values measured by most radars. The coupling between states is given in (4.7) involving the matrix (4.9a)

$$M_{\nu\nu\prime} = i(\underline{e}_\nu \phi \dot{\underline{e}}_{\nu\prime}) \tag{7.1}$$

By taking the time derivative of (3.2) and using the orthonormality condition (3.8) we can reexpress this as

$$M_{\nu\nu\prime} = i \frac{(\underline{e}_\nu|\dot{n}\phi\underline{e}_{\nu\prime})}{\lambda_\nu - \lambda_{\nu\prime}} \tag{7.2}$$

where

$$(\underline{e}_\nu|\dot{n}|\underline{e}_{\nu\prime}) \equiv \int dx \underline{e}^*_\nu(xt) \bullet e_{\nu\prime}(xt) \frac{dn}{dt}(x,t) \tag{7.3}$$

The free modes have a continuum of eigenvalues $\lambda_\nu(t)$ in an infinite space and so we can parameterize them directly in terms of their eigenvalue λ:i.e., $\underline{e}_\lambda$ (x,t). The free modes receive from or give energy to localized states and are driven directly by the heater E_0. In the following we will consider in detail the coupling to a unique

collapsing state denoted by the subscript zero. The equation of motion for the amplitude h_λ of a given free mode then follows from (4.7) as

$$i\,\dot{h}_\lambda + (\omega_0 - \lambda)h_\lambda + \int d\lambda' M_{\lambda\lambda\prime} h_{\lambda\prime} = -M_{\lambda\lambda_0}\, h_0 \; + \; E_0 \bullet (e_\lambda|n) \tag{7.4}$$

Here

$$M_{\lambda\lambda_0} \; = \; i \frac{(\underline{e}_\lambda|\dot{n}|\underline{e}_{\lambda_0})}{\lambda - \lambda_0(t)} \tag{7.5}$$

The third term on the left hand side of (7.4) involving $M_{\lambda\lambda\prime}$ involves the scattering of one free mode from another. By considering the equation for

$$(d/dt) \sum_\lambda |h_\lambda(t)|^2$$

it is easy to see that the scattering terms do not change the total free mode energy while the terms on the right hand side of (7.4) do.

We have explored the details of the free mode radiation in the spherical scalar model discussed in Section 4. The numerical solution of (7.4) can be broken into two parts. First, for given $\lambda > 0$, calculate the associated eigenfunction and matrix elements M; second, choose an appropriate discretization of the integral over λ. In three dimensions it is convenient to work with $\Psi \equiv r\, e_\lambda$, which satisfies (for the scalar model)

$$\lambda\Psi \; = \; -\frac{d^2\Psi}{dr^2} \; + n(r)\Psi \; . \tag{7.6}$$

There are two linearly independent solutions which may be taken as having either unit value or slope at r=0. In order that e_λ have finite $\int |\nabla e_\lambda|^2$, the solution for Ψ with unit value is inadmissable. Except for overall normalization, for given n (r,t) (7.6) is integrated out from $\gamma = 0$ with $\Psi(0) = 0, d\Psi/dr(0) = 1$. Note that for kr large enough such that $n(r) << \lambda$, $\Psi(r) \sim \sin(kr + \delta)$ where $k^2 = \lambda$ and δ is the so called phase shift which depends on n. Therefore $e_\lambda \sin(kr + \delta)/r$ for r large. This is the form expected from scattering theory where δ determines the "S matrix" and everything that you know about scattering. For our purposes, however, the detailed variation of $e_\lambda(r)$ for r small enough such that n matters is required to calculate M.

To determine the optimal choice of discrete λ it is useful to think of the caviton sitting in the center of a very large sphere of radius R, with the boundary condition e_λ (r=R) = 0. It can be shown that the density of states at eignevalue λ, $\rho(\lambda)$, satisfies

$$\rho(\lambda) \sim \frac{1}{2}\frac{R}{\sqrt{\lambda}} + \frac{d\delta}{d\lambda} . \tag{7.7}$$

For large enough R the density of states is indistinguishable from the case of (7.6) with n = 0. That is, the discrete set of positive eigenvalues is λ_0 $4\lambda_0$, $9\lambda_0$, $\cdots$ where $\lambda_0 = (\pi/R)^2$. With this choice of states, a consistent normalization is

$$4\pi \int_0^R r^2 e_\lambda^2 \, dr = 1 . \tag{7.8}$$

For large R, this integral is dominated by regions of space where n is ignorable, and then

$$e_\lambda(\vec{r}) \sim \frac{\sin(k\vec{r}+\delta)}{r\sqrt{R}} . \tag{7.9}$$

It can be shown that the discretization of (7.4), under the transformation $\lambda_0 \to \lambda_0/4$ (equivalently, R $\to$ 2R), transforms in such a way that the energy density of the free modes (the amount of energy in the free modes per unit λ) is invariant in the limit where R is large, so that this choice of discretization should converge to the exact solution of (7.4) in the limit of $\lambda_0 \to 0$.

A complete specification of the numerical method must also include the largest free mode eigenvalue considered, λ_{max}. On physical grounds, the coupling between a very energetic free mode and the collapse process should be weak. Numerical convergence is indicated when, for fixed λ_0, increasing λ_{max} has only a small effect on the total evolution, and for fixed λ_{max}, a decrease in λ_0 has little effect. This is the case for the data presented in Figures 19.

We turn now to some results from these numerical studies. During the first part of nucleation, there is relatively little energy, $|h_0|^2$, in the local ground state, e.g., see Figure 19c and the coupling of the heater, (the last term on the right hand side

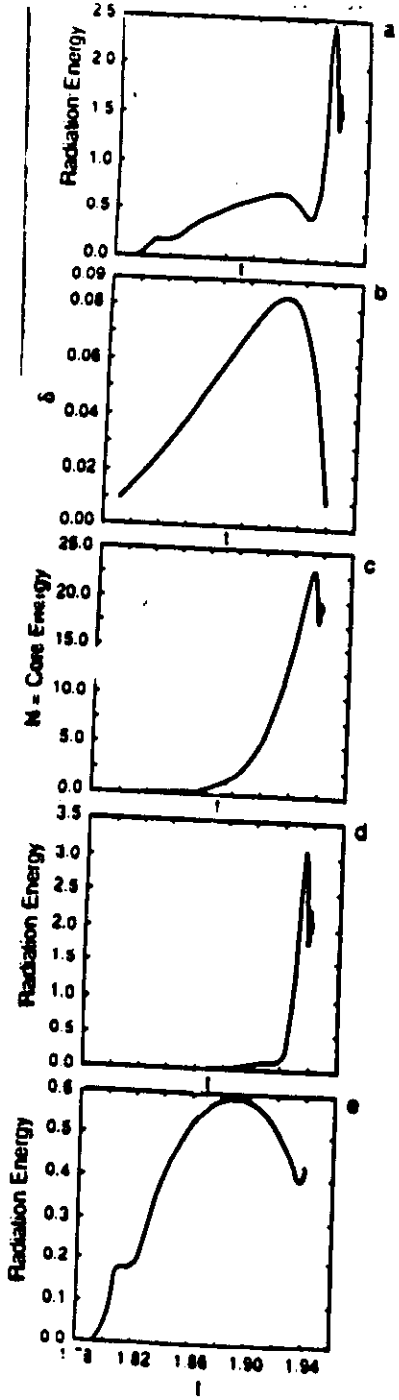

Fig. 19

a. Evolution of energy in free modes, $\int d\lambda |h_\lambda|^2$ for the scalar calculation. $E_0 = 5.0$, $\omega_i = 0.8$, $\omega_0 = -40.0$, $m_r/\eta m_c = 20{,}000$.
b. Evolution of the width of the ground state.
c. Evolution of the energy in the ground state.
d. Evolution of energy in the free modes without the dynamic con term $E_0(e_0|n)$ in (10.4).
e. Evolution of energy in the free modes without the time depe coupling to the ground state M_{n0} in (10.4).

of (7.4), is the dominant source of free mode energy. This coupling is a dynamic generalization of direct conversion, and so we call it dynamic conversion. Deep into collapse, coupling to the ground state is again unimportant because the coupling coefficient is going to zero and the coupling is more and more nonresonant. At intermediate times during collapse the ground state coupling is dominant.

To determine which source term is overall most important, the scalar local nucleation model was used to calculate all the terms in (7.4) for the case of an overdense plasma with parameters M_i/M_e = 20,000, E_0 = 5.0, ν_i = 0.8, ω_0 = −40.0 In Figure 19a the evolution of the total energy in the free modes, $\int d\lambda |h_\lambda|^2$, is shown, while in Figures 19b and 19c the evolution of the ground state parameters is shown. Since the energy in the free modes is a small fraction of the collapsed energy, the coupling of the free modes in the equation of motion for h_0 was ignored. In Figure 19d for the same collapse as in Figures 19a-c, the evolution of the free mode energy is shown without the dynamic conversion source term, while in Figure 19e the free mode energy is shown with the ground state coupling term removed from (7.4). We see that the coupling to the time dependent collapsing Langmuir ground state mode is the dominant source of Langmuir wave radiation, at least in the case of an overdense plasma.

In reference 1 we have also shown that the hot electrons emitted in the burnout phase of collapse do not produce a significant rate of free Langmuir wave radiation by Cerenkov radiation. Thus it is the wave-wave coupling of the collapsing field to the nearly free Langmuir waves which is the dominant source of free mode emission.

In the experiments of Cheung et al. [1989], the ratio of the strength of the "collapse continuum" portion of the spectrum for $\omega < \omega_0$ to the strength of the free mode line increases as the time delay following the onset of the heating increases. It is observed that the strength of the free mode line does not change by as much as an order of magnitude while the strength of the collapse continuum increases by several orders of magnitude. This is consistent with the increase of the $\omega < \omega_0$ spectrum due to the onset of correlations, i.e., a signal proportional to N_c^2 rather than N_c. The free mode line is not strengthened by correlations except in the unlikely case that the free mode peak at $\omega = \omega_f$ in the single caviton spectrum coincides with one of the correlation peaks at $\omega = 2\ nm/\tau_c$, which were discussed in Section 8. In addition, we know that free mode emission is weaker from overdense regions where $\omega_0 < 0$ which are likely to be correlated. Note, for example, that

the free mode peaks in the single caviton spectra from the correlated simulations of Figure 14 where $\omega_0 = -25$ are not very strong and do not produce prominent peaks in the correlated spectra.

11. CONCLUSIONS

A goal of this research has been to explore in detail the implications of strong Langmuir turbulence theory for ionospheric heating experiments. The short time scale data from these experiments provide the best test of the theory available today. A major conclusion of our work is that weak turbulence theory (WTT) cannot be valid for the conditions of ionospheric heating. Our conclusion is based, first of all, on extensive numerical solutions of Zakharov's model encompassing many generations of collapsing cavitons. WTT follows under very special conditions from the Zakharov equations. The fact that the numerical solutions are dominated by coherent, collapsing cavitons proves that the nonlinear state is far from the regime of WTT. Recently Payne, Nicholson and Shen[26] have explored in detail the limit of WTT in numerical solutions of Zakharov's equations in one dimension and have established rough criteria for the validity of WTT. These stringent criteria are not satisfied for the conditions of ionospheric heating.

The strong Langmuir turbulence theory has developed on two levels. The first level is based on solutions of Zakharov's model equations. From the properties of these solutions we have proposed the local caviton model which is a more "phenomenological" level. The local caviton model is built on single caviton properties. Cavitons go through cycles of nucleation, collapse and burnout. Associated single caviton properties include their lifetimes (or cycle times) τ_c, the single caviton field fluctuation $\mathcal{E}(\underline{x},t)$ and its power spectrum $|\mathcal{E}(k,\omega)|^2$. These single caviton properties are not necessarily those of isolated cavitons, although the isolated caviton approximation is at least qualitatively useful in many cases. As the driving becomes increasingly overdense ($\omega_0 < 0$) we have evidence that caviton interactions decrease but the residual interactions can lead to coherent caviton states. It is a great challenge to understand the mechanism(s) for self-organization of this weakly interacting caviton gas. For these highly correlated states, the name turbulence hardly seems appropriate.

We believe that the qualitative properties of the local caviton model will be

those deduced from the Zakharov model. More complete and accurate descriptions of single caviton properties are needed to treat the end stages of collapse and the burnout processes, whereas the nucleation and early collapse stages should be accurately described by the model. We anticipate that these improvements will make quantitative but not qualitative changes in the picture developed in this paper.

We believe that the SLT model has at least three apparent successes in explaining the ionospheric heating data:

1.) The altitude dependence of the plasma line signal[36,37] is easily explained because the localized caviton states are not tied to the linear dispersion relation, (2.5). Based on the sensitive dependence of the turbulence level on E_0 we concluded that the strongest plasma line signal should occur near the altitude of strongest E_0, which is the first Airy maximum in an undisturbed profile.

2.) The angular dependence of the SLT spectrum is at about two orders of magnitude more isotropic than WTT predictions.[38,39] Therefore, there is no problem in understanding the strong signals observed at Arecibo where k is at 45° to B_0 and the fact that the observed long time spectra at Tromsøwhere $\theta < 18°$ is not qualitatively different than at Arecibo. The sharp spectral features, which we associate with correlations, can occur in the SLT theory for $\theta = 45°$ as well as for $\theta \simeq 0$.

3.) The short time scale spectra observed by Wong et al.[12], Djuth et al.[13] and Cheung et al.[14] can be explained in detail by SLT. This includes a new prediction of SLT, the free mode peak, which results from the radiation of Langmuir waves from collapsing cavitons [Cheung et al.[14]]. The broad featureless spectrum for $\tilde{\omega} < \tilde{\omega}_H$ is explained by the dynamics of the local caviton cycle. None of these features is explained by WTT.

The success of SLT in explaining these short time scale results leads to the conclusion that if SLT is to explain the sharp spectral features observed on a long time scale that cavitons must evolve to a state with strong spatio-temporal correlations. Single radar pulse data obtained by Cheung et al.[14] are consistent with strong temporal correlations even at relatively early times after the onset of heating. We have postulated correlated caviton models which predict that when spatial Bragg resonance conditions which depend on the radar k, are satisfied that sharp spectral

features including the "decay line" the 3:5:7: --- "cascade lines," the "anti-Stokes" line and the "OTSI line" are present in the spectrum. The possibility of very narrow lines[34,35] such as the "OTSI line" emerges as a result of very long lived caviton cycles.

At this stage we can only make preliminary guesses as to how such correlated caviton states could develop. We believe that overdense regions of relatively high heater strength are necessary to obtain strong temporal correlations. The question of how spatial correlations develop in such regions is completely open. We do know that initially correlated states in such regions can be very stable and have been able to set up such states which lead to spectra very similar to the postulated strongly correlated models. In such regions the spacing of an ordered array of cavitons is expected to decrease as E_0^{-1} which led us to conclude that the lowest order Bragg resonance condition can only be satisfied for relatively strong E_0 and that this might explain why the sharp featured spectra are the strongest spectra.

In situ rocket or satellite diagnostics in the heated ionosphere appear to be the most direct way to observe the presence of Langmuir energy in the form of localized cavitons. Perhaps even correlation properties could be measured.

The problem of fast (or hot) electron generation in collapse and the airglow excited by these electrons is a problem at the frontier of this subject. The recent airglow experiments of Bernardt, Duncan and Tepley[40] give increased incentive for a more complete understanding of the flux and energy distribution of hot electrons. As discussed in Section 10, in regard to Cerenkov emission from hot electrons, we believe that the model discussed in this paper can give fairly accurate values for the hot electron flux but allows no estimate of the energy distributions. Kinetic (PIC) simulations and transit time damping calculations can provide information here. This is a topic for future study.

As mentioned in Section 5, density compression regions associated with irregularities excited by thermal instabilities might be the source of the postulated overdense domains in which cavitons are correlated. The coupling of the small scale Langmuir turbulence to the larger scale thermal fluctuations is another important area for new research.

These questions are a challenge for future work. We believe that the new strong Langmuir turbulence model presented here is considerably more successful

in describing the early-time behavior of the heated ionosphere than the conventional theory. We hope this paper will stimulate new experimental and theoretical tests of these ideas.

ACKNOWLEDGMENTS

We are grateful to Drs. P. Y. Cheung, T. Tanikawa, J. Santoree and A. Y. Wong for permission to discuss and present their unpublished experimental results. This research was supported in part by the U.S. Department of Energy, the Office of Naval Research, the Los Alamos Center for Nonlinear Studies and the Institute for Geophysics and Planetary Physics.

REFERENCES

1. D. F. Dubois, H. A. Rose and David Russell, Excitation of Strong Langmuir Turbulence Near Critical Density: Application to HF Heating of the Ionosphere, Los Alamos National Laboratory Report LA-UR-89-1419 (to be published).

2. V. E. Zakharov, Collapse of Langmuir waves, Sov. Phys. JETP, 35, 908, 1972.

3. D. Russell, D. F. DuBois and H. A. Rose, Nucleation in Two-Dimensional Langmuir Turbulence, Phys. Rev. Lett. 60, 581-584.

4. D. F. DuBois, Harvey A. Rose and David Russell, Power spectra of fluctuations in strong Langmuir turbulence, Phys. Rev. Lett. 61, 2209, 1988.

5. P. A. Robinson, D. L. Newman and M. V. Goldman, Three dimensional strong Langmuir turbulence and wave collapse, Phys. Rev. Lett. 61, 702, 1988.

6. G. D. Doolen, D. F. DuBois and H. A. Rose, Nucleation of cavitons in strong Langmuir turbulence, Phys. Rev. Lett. 54, 804-807, 1985.

7. D. Russell, D. F. DuBois and H. A. Rose, Collapsing caviton turbulence in one dimension, Phys. Rev. Lett. 56, 838-842, 1986.

8. H. A. Rose and M. I. Weinstein, On the bound states of the nonlinear Schrödinger equation with a linear potential, Physica D, 30, 207-218, 1988a.

9. A. A. Galeev, R. Z. Sagdeev, Yu S. Sigov, V. D. Shapiro, and V. I. Shevchenko, Nonlinear theory for the modulational instability of plasma waves, Fiz. Plazmy 1, p 10, 1975 [Sov. J. Plasma Phys. 1 p 5, 1975].

10. H. A. Rose, D. F. DuBois and B. Bezzerides, Nonlinear Coupling of Stimulated Raman and Brillouin Scattering in Laser-Plasma Interactions, Phys. Rev. Lett. 58, 2547-2550, 1987.

11. H. A. Rose, D. F. DuBois, David Russell, and B. Bezzerides, Experimental signatures of localization in Langmuir wave turbulence, Physica D 1988b.

12. A. Y. Wong, G. J. Morales, D. Eggleston, J. Santour, and R. Behnke, Rapid conversion of electromagnetic waves to electrostatic waves in the ionosphere, Phys. Rev. Lett. 47, 1340, 1981.

13. F. T. Djuth, C. A. Gonzales and H. M. Ierkic, Temporal evolution of the H-F-enhanced plasma line in the Arecibo F region, J. Geophys. Res. 91, p 12,089-12,107, 1986.

14. P. Y. Cheung, A. Y. Wong, T. Tanikawa, J. Santoree, D. F. DuBois, Harvey A. Rose, and David Russell, Short time scale evidence for strong Langmuir turbulence in H-F heating of the ionosphere, (submitted to Phys. Rev. Letters, 1989).

15. J. C. Weatherall, J. P. Sheerin, D. R. Nicholson, G. L. Payne, M. V. Goldman, and P. J. Hansen, Solitons and ionospheric heating, J. Geophys. Res. 87, 823-832, 1982.

16. V. E. Zakharov and L. N. Shur, Self similar regimes of wave collapse, Sov. Phys. JETP 54, 1064, 1981.

17. A. I. Dyachenko, V. E. Zakharov, A. M. Rubenchik, R. Z. Sagdeev and V. F. Shvets, Two dimensional Langmuir collapse and two dimensional Langmuir cavitons, Pis'ma v ZhETF 44, 504 (1986) [JETP Letters, 44, 648, 1986].

18. A. I. Dyachenko, A. M. Rubenchik, R. Z. Sagdeev, V. F. Shvets, and V. E. Zakharov, Computer simulation of the Langmuir collapse of the isolated cavity in Plasma Theory and Nonlinear and Turbulent Processes in Physics, Vol. 2, ed. by V. G. Bar'yakhtar et al., World Scientific 1987.

19. C. Aldrich, B. Bezzerides, D. F. DuBois and H. A. Rose [1984 unpublished].

20. V. E. Zakharov, A. N. Pushkarev, A. M. Rubenchik, R. Z. Sagdeev and V. F. Shvets, Final stage of 3D Langmuir collapse, JETP Lett. 45, #8, 287 (1988) [Pis'ma Zh. Eksp. Teor. Fiz. 47, #5, 239 (1988)].

21. B. D. Fried, and R. W. Gould, Longitudinal ion oscillations in a hot plasma, Phys. Fluids 4, 139 (1961).

22. D. F. DuBois and M. V. Goldman, Radiation induced instability of electron plasma oscillations, Phys. Rev. Lett. 14, 544, 1965.

23. A. A. Vedenov and L. I. Rudakov, Interactiono of waves in continuous media, Sov. Phys. Dokl. 9, 1073 (1965).

24. K. Nishikawa, Parametric excitation of coupled waves. I. General formulation, J. Phys. Soc. Japan, 24, 916-922, 1968a, and Parametric excitation of coupled waves. II. Parametric plasma-photon interactions, J. Phys. Soc, Jap. 24, 1152-1158, 1968b.

25. D. R. Nicholson, Plasma Theory, John Wiley & Sons, N.Y., 1983.

26. G. L. Payne, D. R. Nicholson, and M. M. Shen, Numerical test of weak turbulence theory, preprint 1989.

27. A. Y. Wong and P. V. Cheung, Three dimensional self-collapse of Langmuir waves, Phys. Rev. Lett. 52, 1222, 1984.

28. F. W. Perkins, A theoretical model for short-scale field aligned plasma density striations, Radio Science, 9, 1065 (1974).

29. A. C. Das and J. A. Fejer, Resonance instability of small-scale field aligned irregularities, J. Geophys. Res. 84, 6701, 1979.

30. K. B. Dysthe, E. Mjølhus, H. Pècseli and K. Rypdal, Thermal cavitons, Physica Scripta, T212, 548-559, 1982.

31. A. M. Rubenchik and S. K. Turitsyn, On self-focusing of laser beams in plasma, Laser and Particle Beams, 5, 3-14, 1987.

32. J. A. Fejer, C. A. Gonzales, H. M. Ierkic, M. P. Sulzer, C. A. Tepley, L. M. Duncan, F. T. Djuth, S. Gangulys, and W. E. Gordon, Ionospheric modification experiments with the Arecobo Heating Facility, J. Atmos. Terr. Phys. 47, p. 1165, 1985.

33. C. Kittel, Introduction to Solid State Physics, 3rd Ed., John Wiley & Sons, N.Y., 1968.

34. M. P. Sulzer, H. M. Ierkic, J. A. Fejer and R. L. Showen, HF-induced ion and plasma line spectra with two pumps, J. Geophys. Res., 89, 6804, 1984.

35. M. P. Sulzer, H. M. Ierkic, and J. A. Fejer, Observational limitations on the role of Langmuir cavitons in ionospheric modification experiments at Arecibo, J. Geophys. Res. (1988).

36. D. B. Muldrew, and R. L. Showen, Height of the HF-enhanced plasma line at Arecibo, J. Geophys. Res. 82, 4793, 1977.

37. T. Hagfors and G. F. Gieraltowski, Stable electron density fluctuations in the presence of a high frequency electric field, J. Geophys. Res. 77, 6791-6803, 1972.

38. F. W. Perkins, C. Oberman and E. J. Valeo, Parametric instabilities and ionospheric modification, J. Geophys. Res. 79, 1478-1496, 1974.

39. J. A. Fejer and Y. Kuo, The saturation spectrum of parametric instabilities, AGARD Conf. Proc., 138, 11-1-11-8, 1974.

40. P. A. Bernhardt, L. M. Duncan and C. A. Tepley, Artificial airglow excited by high-power radio waves, Science 242, 1022-1027, 1988.